Metal Mimics: Lightweight, Strong, and Tough (Nano)Composites and Nanomaterial Assemblies

Adam J. Clancy,[a]* David B. Anthony,[b] Francois De Luca[c]

a) Department of Chemistry, University College London, London, WC1E 7JE, U.K.
b) Department of Chemistry, Imperial College London, SW7 2AZ, U.K.
c) National Physical Laboratory, Teddington, TW11 0LW, U.K.

*Corresponding author, email: a.clancy@ucl.ac.uk

Keywords: Composite, nanomaterials, toughness, carbon nanotube, graphene, nanotechnology, nacre, nanotube yarn, supracrystal, carbon fibre

Abstract

The ideal structural material would be high strength and stiffness, with a tough ductile failure, all with a low density. Historically, no such material exists, and materials engineers have had to sacrifice a desired property during materials selection, with metals (high density), fibre composites (brittle failure), and polymers (low stiffness) having fundamental limitations on at least one front. The ongoing revolution of nanomaterials provides a potential route to build on the potential of fibre-reinforced composites, matching their strength while integrating toughening behaviours akin to metal deformations all while using low weight constituents. Here, the challenges, approaches, and recent developments of nanomaterials for structural applications are discussed, with an emphasis on improving toughening mechanisms – often the neglected factor in a field which chases strength and stiffness.

1. Introduction

High performance continuous fibre reinforced-polymer (FRP) composites revolutionised the materials landscape in the 1960's onwards, coupling unparalleled strength and stiffness with low density, allowing innovation in the fields of aerospace, civil engineering, and automotive, amongst many others. However, these materials intrinsically suffer from brittle, catastrophic failure at low strains, leading to limited energy absorption before/during failure – i.e. low toughness. In the high-stress environments in which high strength and stiffness materials (including FRPs) are used, higher toughness is highly desirable to extend lifetime, reduce required engineering safety margins, and facilitate damage monitoring.[1] Historically, the only materials class to couple this high toughness to high strength/stiffness were structural metals,[2] which are inescapably dense, lowering specific mechanical properties, hampering their use in many applications (Figure 1). Resultantly, there is a need for materials which can combine the toughness/ductility and strength of metals, while maintaining low density to give higher specific (i.e. weight normalised) strength, stiffness, and toughness.

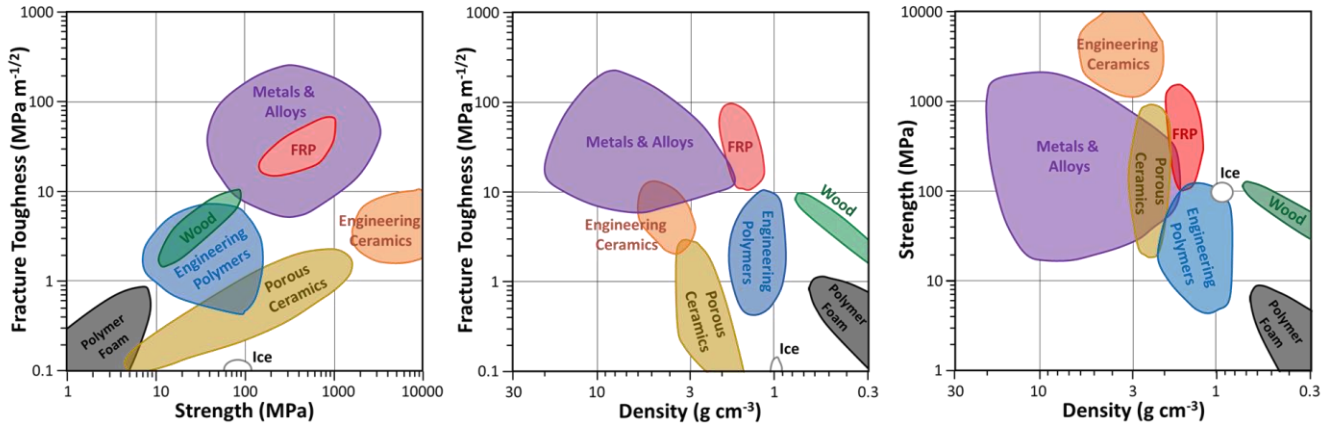

Figure 1. Material property Ashby charts comparing families of materials with values taken from *Materials Selection in Mechanical Design* by M. Ashby.[2] Note that abscissas (density) has been inverted for middle and right chart, to produce Ashby charts in which the top right hand side projects towards the idealised material properties in each instance.

This review covers the research into increasing toughness in high strength/stiffness materials, predominantly through the use of nanomaterials. Section 2 will briefly cover the background, touching upon high performance composites and utility of nanomaterials, as well as the main toughening mechanisms and how these behaviours are most commonly monitored. Section 3 will discuss how tougher versions of standard composites have been created, covering both nanocomposites and FRPs modified with nanomaterials to

create multiscale composites. Section 4 will discuss architectures of nanomaterials beyond dispersion in a continuous matrix, notably brick and mortar 'nacre-like' assemblies, nanomaterial papers, yarns, and supracrystals, before providing the authors' outlook for the field in Section 5.

2. Materials Background

An important starting point is to consider why a material or combination of materials are chosen for a specific purpose or use. Composite materials, two complimentary materials which when combined produce a material with at least one improved property, commonly consisting of a filler (reinforcement) and matrix (surrounding medium),[3] are dominant in material science due to their synergistic nature. The properties of the filler, matrix, architecture, the filler-matrix interface and deformation/damage tolerance of the constituents all play a part in determining the material's toughness, while the direction of applied stress (tensile, shear, compressive), and the relative direction versus anisotropic components/defects/existing cracks will also alter the failure mechanics and the measured toughness. This complexity also provides avenues to tailor responses as discussed in the following sections.

2.1. Fibre Reinforced Polymer Composites

In FRPs, stress transfer between the stiff filler (i.e. fibres) is ensured through the interface with the (softer) matrix, in shear. The mechanical response of the composite can be predicted by the so-called Rule of Mixtures (RoM), with modulus (E_Y) and stress (σ) in the direction of fibre orientation scaling linearly with filler fraction. With a strong interface between the matrix and the filler and at sufficiently high aspect ratio, the fillers can carry high stress, facilitating high composite strength, and are the first component to fail. Upon failure, local stress is transferred to the neighbouring fillers through shearing of the matrix. The main fibres of use are carbon fibre (CF, σ 3.5 – 5.5 GPa, E_Y 220 – 450 GPa, ρ ~1.8 g cm^{-3}, diameter (d_f) 5 – 8 µm)[4] and glass fibres (σ 2.4 – 4.6 GPa, E_Y >70 GPa, ρ 2.1 – 2.6 g cm^{-3}, d_f 1 - 25 µm)[5] which are most commonly embedded in a thermoset matrix such as epoxy or polyester. The main disadvantage of high strength carbon fibre reinforced-polymers is their lack of toughness - the energy absorbed by the material during fracture - as bond cleavage and plastic deformation are limited by the sudden rupture of the material. When tensile stress is applied to the composite, the fracture of individual fillers in high strength and brittle materials typically triggers critical straight propagating cracks due to the high local stress concentration, leading to a catastrophic failure of the material caused by local accumulation of damage after limited deformation.[6] The brittleness of the failure is

also linked to a more variable lifetime,[7-8] leading to more regular replacement or over-engineering of a given component. Under compression, the effect is exacerbated by the lower compressive properties of many reinforcing fibres, debonding leading to fibre fracture and kink band formation.[9] To increase toughness, more bonds must be broken e.g. cracks can be deflected/blunted to increase the crack pathway required to fracture the material. Tougher matrixes may be used such as thermoplastics (e.g. polyether ether ketone which has 50 – 100 times higher fracture toughness than epoxies)[3] or low aspect ratio fillers/weak interfaces may be used to cause failure at the interface[10] leading to additional toughening mechanisms, notably pull-out (Section 2.3.3), at the expense of composite stiffness and strength.

2.2. Mechanical Benefits of Nanomaterials

The outstanding mechanical behaviour of nanomaterials has long been one of their most appealing properties and is certainly one of the most studied. By scaling down the dimensions of a given material, according to the "Griffith criterion", a high theoretical strength can be achieved as the material becomes flaw-tolerant.[11] At the nanometre length scale, the absolute proportion of defects in a material is significantly reduced, allowing for the "defect-free" ideal strength to be reached, higher than the known "bulk" strength. This inverse trend between sample/element size and (average) strength is well established across a range of length scales, although it should be noted that the variability of mechanical properties also increases.[8, 12] While the proportion of defects decrease, the impact of a given defect is greater on smaller elements leading to greater statistical variation between samples.

Of particular note are the nanocarbons, based on the parent 2D graphene consisting of an atomically thin sheet of sp^2 hybridised carbons in a hexagonal array. Graphene itself is one of the strongest[13] (σ 130 ± 10 GPa at 25% strain), stiffest (E_Y 1.0 ± 0.1 TPa), and highest surface area (2630 $m^2\ g^{-1}$ theoretical) materials known, although it is difficult to create high quality graphene in bulk. Graphene may be oxidised to graphene oxide (GO) which is significantly easier to process, as introduced oxygen functional groups facilitate simple solution processing, however, mechanical (and optoelectronic) properties are severely diminished compared to the parent graphene. GO may be subsequently reduced to reduced graphene oxide (rGO) to partially restore the intrinsic properties of graphene,[14] although the removal of basal plane carbons to form vacancy defects has a severe impact on strength and stiffness.[15] Pristine graphene may conceptually be wrapped into seamless cylinders to give a single-walled carbon nanotube (SWCNT), which itself may be stacked concentrically to give

carbon nanotubes (CNTs) with multiple walls. The hexagonal sp^2 motif may be seen in hexagonal boron nitride and its nanotube analogue which have been used for mechanical reinforcement,[16] albeit to a much lesser degree than the carbon allotropes.

Ceramics provide high strength and stiffness materials with intermediate densities (ca. 2 – 5 g cm^{-3}) similar to light metals (Al, Ti), but have low toughness failure mechanisms (Figure 1). High aspect ratio ceramic nanomaterials may be formed either from exfoliation of ceramics intrinsically consisting of low dimensionality motifs – most commonly as 2D layers (e.g. layered double hydroxides), although intrinsically 1D ceramics (e.g. imogolites) are known – or they may be grown with facet capping to provide controllable high aspect nano/mesoscale species of high aspect ratio species.[17]

Cellulose nanocrystals/nanofibrils have attracted much attention as a bio-based, biodegradable nanomaterial with promising mechanical applications. Cellulose in nature used in a structural capacity is arranged hierarchically into crystalline regions separated by disordered regions across a range of length scales, with a wood fibril consisting of bundles of cellulose nanofibrils (d_f 5 – 20 nm, length 2 – 10 µm), themselves consisting of nanocrystals (d_f 3 – 20 nm, length 0.1 – 1 µm), themselves consisting of cellulose molecular chains. The highly crystalline nature of these cellulose chains leads to high intrinsic strength[18] (7.5 GPa) of the cellulose nanocrystals.

In spite of the high intrinsic mechanical properties of many of these nanomaterials, their high surface energies[19] often lead to a high degree of stacking/bundling/agglomeration, forming aggregates with inferior mechanical properties due to the comparatively weak inter-species bonds. The most famous example is graphene which alone fails through rupture of strong homogenous sp^2 hybridised covalent bonds. However, when stacked to form graphite, it can fail through breaking of the interlayer van der Waals (vdW) bonds which have a slippage energy[20] of only 0.37 J m^{-2}.

2.3. Toughness and Failure Mechanisms

The concept of toughness is simply the measurement of energy absorbed through deformation under an applied force without material failure. While comprehensive, this definition is necessarily vague, with the ability of a material to absorb energy before and during failure governed by its material constituencies and the interface between them, defects, construction/architecture, order, and the mechanism(s) of failure. Given the nature of deformation, there is no single metric.

The ability of a material to resist the deformation, arrest/limit damage onsets can be tailored in a bid to alter their toughness. Modifications to alter the constituent's interface, alter the failure path, or diffuse damage sites are the most common approaches, with nanomaterials as previously discussed a common additive filler. The absorption of energy in a material under deformation is always linked to the breaking of bonds. The more bonds which must be broken, and the stronger those bonds, the higher the total amount of energy must be applied before failure, and thus the stronger the material. There are many types of bonds, with varying strength, such as covalent < ionic < dipole < hydrogen-bonding < physisorption, altering the overall capacity of the system to absorb energy. In real systems, most failures will involve multiple mechanisms during the failure procedure.

2.3.1. Polymer Deformation

The failure mechanics of polymers is a broad field, in part due to the large range of parameters including, but not limited to, polymer intrinsic structure (linear, branched, crosslinked), backbone/crosslink chemistry and heterogeneity, polymer molecular weight and dispersity, presence of additives/plasticisers, mesoscale arrangement (lamellae, spherulite, entanglements), degree of crystallinity, and temperature of the polymer during failure, particularly with reference to the glass transition. In general, however, there are three deformation mechanics which are important for understanding the origin of high toughness in polymers: chain slippage, crazing, and chain scission.

Chain slippage is the predominant deformation mechanism of amorphous polymer regions at temperatures above the glass transition, and unfolding crystalline regions in semicrystalline polymers.[21] The polymer chains can move past each other to reorient and align along the shear direction, so long as there is no constraint on chain mobility normal to the applied stress (e.g. not under triaxial stress). The vdW interactions between adjacent chains are broken before reforming once chain motion has ceased. The shear alignment tends to increase the per-polymer strength of the interactions and (re)crystallisation may occur, although a concurrent reduction in cross-section often leads to a perceived plateau in stress in 'necking' behaviour. The weak nature of the bonds being broken leads to a low stress deformation, but when maintained over large feasible strains, can lead to high total energy absorption. Use of high strength interchain bonding, e.g. hydrogen bonding in poly(vinyl alcohol), can substantially increase strength without sacrificing a substantial degree of toughness.

Crazing is a brittle failure mechanism seen in polymers with long/stiff chains with low entanglement density at low temperature. Under stress, nanoscale voids form which are bridged by extended polymer chains/fibrils perpendicularly bridging the gap, allowing the region to continue carry load (Figure 2). By reinforcing the region, it prevents the craze forming an abridged crack which would otherwise propagate, leading to fracture. The delay allows other areas of the polymer to undergo deformation under stress allowing greater energy absorption in the material, although the total deformed area is typically lower than chain slippage mechanisms which involve a higher total volume of material being deformed.

Finally, covalent bonds may be cleaved in chain scission, which is the predominant failure mechanism in glassy ($T < T_g$) and crosslinked thermoset polymers. Here failure through chain rupture is required, and the energy absorbed is related to the broken bonds, and the number which must be broken. While key for maximising polymer strength and stiffness, these processes tend to lead to failure at low stresses with few bonds being involved in the deformation/fracture, translating into lower toughness than other polymer failure mechanisms.

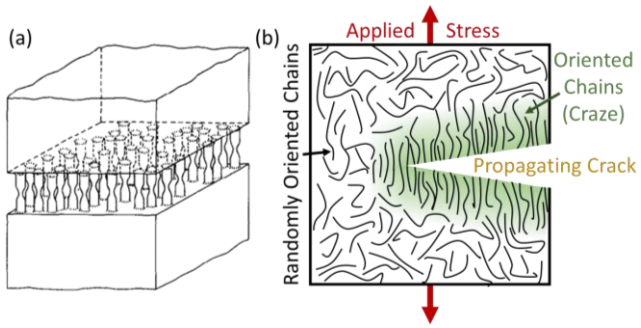

Figure 2. Schematics of polymer crazes. (a) Craze fibril structure, reproduced with permission from Passaglia.[22] Copyright 1987 Elsivier. (b) Polymer orientation at craze and after crack propagation through crazed region.

While weaker on a per-bond basis than other components in composite systems, the high number of bonds which may require breaking during polymer deformation leads to a significant contribution towards the total energy absorption. Resultantly, maximising polymer deformation is one of the most commonly targeted routes to improving composite toughness. Mechanisms such as crack deflection/arrestment and limiting stress concentrations are often used predominantly to maximise the number of polymer bonds which must be broken within the matrix. The use of stronger polymers within a composite may increase the per-bond strength, however, care must be taken to ensure that matrix failure still proceeds through these non-brittle mechanisms to ensure the material toughness is increased.

2.3.2. Filler Failure

In a stiff-filler composite, if the filler is longer than a critical length (l_c), the filler may fracture. This critical length is dependent on the strength of the filler material (σ_f), the interfacial shear strength (τ_i), and the geometry of the filler (diameter, d_f, for uniaxially strained 1D materials such as fibres) as described in Equation 1,

$$l_c = \frac{\sigma_f d_f}{2\tau_i} \quad . \tag{1}$$

Alignment and orientation of anisotropic stiff and strong fillers in the bulk matrix alters the efficiency of the toughening response.[23] Although the anisotropy of the resultant composite arises,[24] when the filler is orientated perpendicular to the failure mode, it can lead to higher toughened responses. When anisotropic stiff and strong fillers lie in the same axis as the crack propagation, the efficiency is reduced.

Typically, failure dominated by filler failure is associated with high strength but low toughness composites. As fractures occur, fillers adjacent to the fractured filler will be subjected to higher stresses and are more likely to fail due to local increase in stress concentrations, leading to a propagation of filler failures, which may culminate with failure of the overall material at limited deformation. While the intrafiller bonds are typically strong in high performance composites, a low number of these bonds are broken during failure, limiting the toughness of the material. Counterintuitively, this means that increasing the interfacial shear strength can lead to lower energy absorption.

Conversely, low-strength bulk matrix fillers (e.g. rubber adduct and preformed core–shell rubber) may be introduced to increase toughness through cavitation and extensive plastic void growth and shear deformation,[25] leading to high energy absorption. However, these plastic filler types tend to lead to significantly lower strengths and stiffnesses than FRCs, even when hybridized.[26-27] Investigations of FRCs containing rubber particles fillers (with/and without hybridisation) are limited but tend to show reduced stiffness/strength but increased toughness.[28]

2.3.3. Filler Pull-Out

The most common mechanism to maximise the toughness of composite materials is the pull-out mechanism, inducing a prolonged failure of a material through distribution of load and more tortuous failure mode. When the interface between the matrix/filler is the weakest point (filler under the critical length), initial failure occurs at this interface and filler pull-out is observed. This mechanism absorbs energy through friction

between the filler and matrix, and deformation of the adjacent matrix as the filler is drawn from the surrounding matrix. If the filler surface is not parallel to the shearing forces, the filler will be dragged through the adjacent matrix causing wedging and ploughing effects, which subsequently increase material deformation and, therefore, increase toughness. By using a roughened surface, these matrix deforming effects may be increased. These toughening processes occur after the failure onset and are located in the process zone generated at, and ahead of, the failure site.

2.3.4. Crack Manipulation

The concept of crack manipulation is simple: the more bonds a crack must break to extend across a material, the greater the total energy which must be expended to break the bonds. The propagation of a crack is dependent on the orientation of the existing crack to the shear force applied (Figure 3), with the toughness varying depending on the Mode of failure. For brittle failure, most energy is absorbed by the energy of the crack surface being formed, however, for ductile materials, the crack edge the proceeding crack forms a plastic zone at the crack tip to deform, with the deformation absorbing significant energy through alternative mechanisms. In a homogenous material, once the threshold for crack formation has been achieved, the propagation of the crack goes unhindered. In systems consisting of more than one phase/filler/pathway, the crack can be arrested or deflected into alterative directions, at interfaces as well as towards matrix/filler rich regions. To maximise the cumulative energy absorption of the crack(s), their propagation may be hindered through blunting or stabilisation (using through polymer chains/fibrils bridging, akin to craze stabilisation, Section 2.3.1), such that new cracks are formed or by increasing the tortuosity of their pathway.

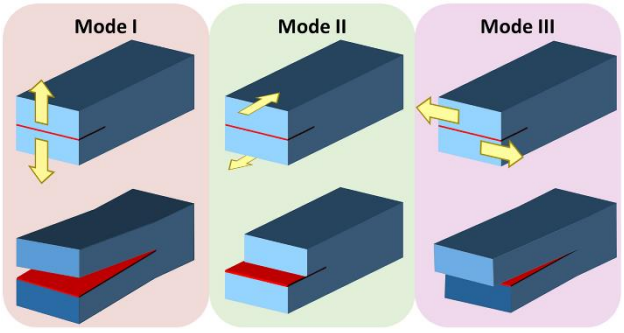

Figure 3. Schematic of crack propagation modes before (top) and after (bottom) applying stress in specific directions (yellow arrows) relative to a pre-existing crack (red). From left to right, Mode I, tensile stress normal to crack plane; Mode II, shear stress perpendicular to crack front; Mode III, shear stress parallel to crack front.

2.3.5. Dislocations

Materials consisting of atomic lattices fail through different mechanisms, and it is these processes which lead to the high strengths and toughness's seen in metals. Above the yield stress of a metal, dislocations within the atomic lattice can move along slip planes until pinned (by grain boundaries, allowing elements, impurities, second phase precipitates, etc.). Hence a higher number of dislocation form at higher stresses, accommodating the plastic flow. The increase in strength from dislocation pinning leads to 'work hardening' of the metal, wherein damage accumulation leads to an increase in the stress required to cause greater deformation.

In contrast to metallic lattices, ionic lattices have remarkably poor mechanical properties, due to their states after plane sliding. Slipping of two adjacent planes leads to adjacent like-charges which repel, forming cracks. The absolute energy required to move the planes per broken bond is high, while the low tortuosity nature of the resultant cracks leads to poor energy absorption, resulting in a strong but low toughness material.

2.4. Testing Toughness

Standard testing methodologies to evaluate material toughness, elude and evaluate individual materials or simple constructs only; factors such as the speed of deformation, type (mode) of shear applied, and normalisation must be considered in idealised cases.

However, constituent toughness values do provide datum input for predictive models, which have advanced significantly in recent years.[29] Extensive virtual testing is now common to pin-point failure points and the processes of failure. Yet, for all the complexities which can be computed, parts still need to be manufactured and tested to determine their failure, such is the variability and dependence on the whole structure rather than the inherent material properties. Difficulties arise when nanomaterials are used to modify systems, as forms or structures often do not conform to these prescribed standard tests. Subsequently, various approaches have been undertaken to determine their effect on toughness.

For macroscopic materials, crack propagation tests are the most accurate route to testing toughness, involving introducing an initial crack and calculating the force required to introduce a given crack area, providing an area-normalised force for fracture toughness (K_c). Given the various Modes of crack propagation (Figure 3), several different tests exist to dictate the applied stress versus crack plane, including double

cantilever beam (Mode I), end-load split test (Mode II), end-notched flexure (Mode II), split cantilever beam (Mode III), and edge crack torsion (Mode III). In each case, care must be taken to select a suitable standard (guidance provided by relevant standards) to ensure appropriate comparison to analogous materials in terms of absolute values and statistical variance. For anisotropic materials, the orientation of the crack, applied stress, and material must be considered in parallel; for example, Mode I failure of FRCs for a crack parallel to the fibre orientation will be different from Mode I failure with a crack perpendicular to the fibres. For newly developed materials, it is common for initial experiments to only create milligram scale samples which does not provide sufficient material to create crack propagation test specimens. As such, the most common routes to characterising their mechanical properties are tensile testing and indentation (Figure 4). In all cases, *in-situ* or *post hoc* imaging of the deformed structure, e.g. though scanning electron microscopy, may be performed for the identification of deformation mechanism (particularly for FRP-based materials), testing of nano-objects, fracture toughness measurement, etc.

Tensile testing involves applying strain to a material at a given rate and measuring its stress response. The test can be done from the millimetre to meter range with modulus (E_Y), ultimate tensile stress (σ_u), strain-to-failure (ε_f), and yield strain/stress (ε_y/σ_y) often recorded to compare material properties. As the sample is initially strained, the early gradient of the stress/strain curve (in the elastic regime) provides the Young's modulus (E_Y, modulus of elasticity, also known as stiffness). Brittle materials such as carbon fibres fail without plastic deformation, typically at low ε_f. In the case of a more ductile material, yielding is observed, resulting in a deflection in the stress-strain curve as deformation transition from elastic to plastic, indicative of material relaxation through energy absorption. After yielding, the material may maintain the applied stress, or continue to require increasing energy to further deform (e.g. work-hardening of steels). In addition to providing a description of the mechanical response, the toughness of a material may be quantified by integrating the area under the stress-strain (plotted as Pa/non-dimensional fractional, respectively) curve, to calculate the work-to-fracture (in J m^{-3}), often referred to in literature simply as 'toughness'. This measurement does not account for creep, nor more complex failure modes which may develop after initial failure onset or under cyclic loading, but does provide ranking when taken within a series. Relatedly, mechanical response is a kinetic and not thermodynamic property, and high strain rates lead to fluctuations in toughness due to altered fracture modes.[30]

Indentation involves the penetration of a well-defined, hard indenter tip (diamond, sapphire, cubic boron nitride, etc.), into the tested material, recording the load and depth simultaneously. The process can be performed at the millimetre (Vicker's test), micrometre (microindentation), or nanometre length scale (nanoindentation), over a wide range of loads. Smooth surface and flat geometry are required at the testing scale. The indenter is first loaded into the material, to a maximum applied load/depth, maintained for a short period of time to monitor creep (viscoplasticity), before unloading. The Oliver-Pharr method[31] can be used to extract the hardness and elastic modulus of the material from the unloading segment of the load-depth (P-h) curve, knowing accurately the indenter area function. For a perfectly elastic material, the unloading curve will match the loading curve. However, differences are seen due to plastic deformation/cracking of the material. For brittle materials, such as ceramics, a value of the fracture toughness can be extracted from the length of the cracks triggered at the edge of the indent imprint. For plastically deforming materials, the degree of plasticity can be measured from the ratio of recovered to total applied energy (area under loading/unloading curves respectively), while quantification of fracture toughness is more challenging.[32] *In-situ* indentation of nano-object such as nanopillar and nanocantilever enables the extraction of mechanical properties at the nanoscale as well as allows for the visualisation of deformation mechanisms.

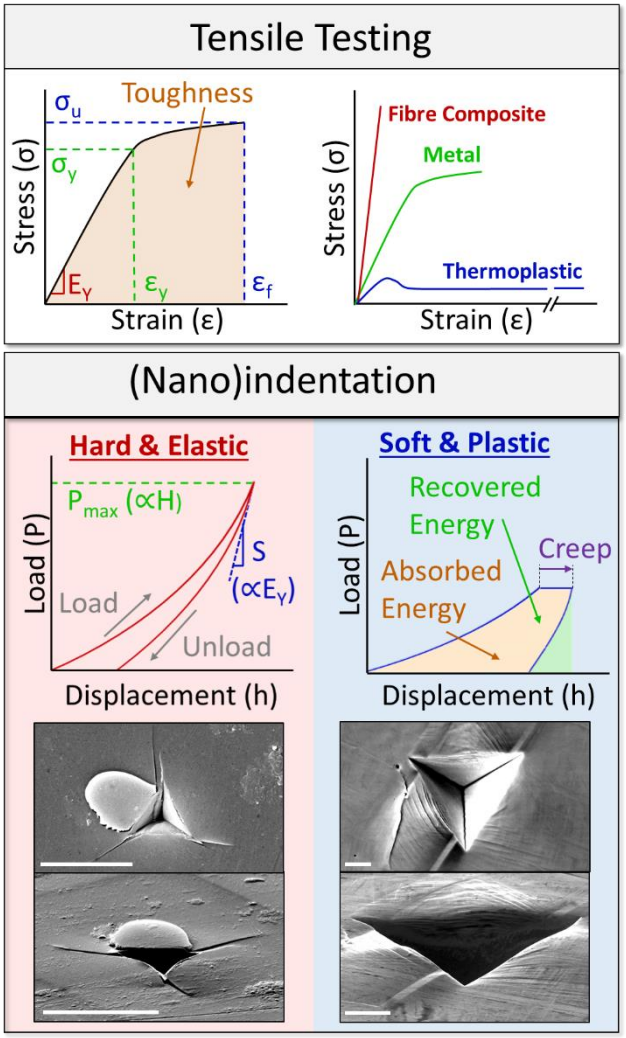

Figure 4. Schematic illustrations of typical mechanical tests for toughness measurements. Top) Illustrative tensile testing stress-strain diagrams: left, showing the values of interest for a strain hardening material; right, showing illustrative curve shapes of various materials. Top) Nanoindentation of (left) brittle elastic and (right) tough plastic materials. Schematic load-displacement curves and representative SEM micrographs of post-indentation fused silica and copper. Scale bars 5 µm.

Care must be taken when comparing the toughness values of materials as tested by nanoindentation or tensile testing versus the better-established crack-propagation values for macroscopic materials. Even for idealised testing, the small samples may lead to both higher maximum values (in keeping with the Griffith criterion) and an increase in the variance in intrinsic properties. Specimens of comparable size after scale-up are not guaranteed to maintain the higher values of the smaller tests. In addition, the lack of standards for testing these new materials provides further uncertainty; differing sample sizes, conformation, normalisation, strain rate, etc. all influencing measured values, complicating direct comparison even with the same

underlying technique. Comparing values derived from differing techniques to rank materials should be avoided if possible.

3. Toughening Classic Composites

3.1. Nanocomposites

Conceptually, nanomaterial fillers represent ideal candidates[33] for the design of high strength and high toughness composites, with outstanding intrinsic mechanical properties, low densities, high surface area to volume ratios, and high aspect ratios. Additionally, many exhibit additional functionalities such as high thermal[34]/electrical[35] conductivities, flame retardancy,[36] and high dielectric constants,[37] which enable the design of multifunctional, mechanically robust materials.

3.1.1. Shear-Mixed Nanocomposites

The straightforward addition of a high-performance nanomaterial to a matrix is the simplest and most sought route to improving the strength and stiffness of a bulk material, an approach which has been reviewed extensively.[38-39] While variations are seen in terms of matrix material (thermoplastic, thermoset, metal, and ceramic), nanoreinforcement dimensionality (0D/1D/2D), length scale (nanometre to centimetre), chemistry, fabrication route, etc., ultimately, the approach is often to mimic the shear-lag behaviour of FRPs at the nanometre length scale. In addition to the benefits in strength and stiffness, introduction of nanomaterials has the potential to dramatically increase the toughness of the bulk material. An increase in toughness is resultant, in part, by the high total surface area of the added nanomaterial; when interfacial failure is initiated it requires many more interfacial bonds to be broken than in conventional FRP composites. Exposing a greater surface area, with the assumption that substantial interfacial debonding occurs throughout the composite, increases the energy absorption, potentially producing more tortuous cracks through the matrix.

Most commonly, nanocomposites are created by mixing the matrix and nanomaterial, aiming to attain a random distribution through a range of routes, including direct shear mixing (commonly extrusion/milling) and shear mixing the nanomaterial into solution before removing the solvent. Shear forces are used to break the initial inter-nanomaterial bonds, although high aspect ratio nanomaterials may be damaged by the process.[40] Other solution phase processes, such as reduction processing[19] or use of intrinsically soluble nanospecies,[41-43] are used, but are nanomaterial-dependent.

Adherence to RoM is usually only seen for very low volume fractions of nanofillers[39] (< 0.1 vol.% for high aspect ratio nanomaterials), with absolute mechanical performance at low loadings dominated by the intrinsic performance of the matrix. At high filler concentrations, nanomaterials agglomerate due to their intrinsic high surface energies.[19] Agglomerates exhibit weak filler-filler vdW interactions, which does not allow for efficient stress transfer to occur through the network of fillers, deteriorating the mechanical performance of the nanocomposite.[39] There is therefore a maximum loading fraction, after which increasing the nanomaterial content diminishes all mechanical properties as the agglomerates begin to dominate the mechanical behaviour.

In thermoplastic matrices, the bulk toughness may drop as the nanomaterials are added at concentrations below the limit where agglomerations limit other properties, due to the high intrinsic toughness of the original polymer. In these systems, the polymer toughness is linked to the high strain-to-failure of both the glassy amorphous and crystalline polymer regions extending and unfolding under low stress, respectively.[21] While the applied force is low, the homogeneity of the bulk polymer facilitates deformation at many sites, leading to failure at a very high strain-to-failure, and subsequently high toughness. While introducing nanomaterials typically increases the stiffness and ultimate tensile stress (strength), the deformation mechanism is altered significantly. During the stresses applied to incur deformation, and after the nanomaterial no longer sustains load from the matrix, e.g. after interfacial failure at the filler/matrix, the (applied) stress may be sufficient to fracture the polymer matrix directly, leading to material failure before polymer chain slippage/elongation is initiated. This premature failure can limit the toughness to a greater degree than the energy absorption gains from the increased strength, reducing the overall toughness.

3.1.2. Controlling Nanofiller Organisation

As discussed in Section 2.3.2, alignment, orientation, individualisation and dispersion of fillers has a significant effect on their reinforcing efficiency and their failure mechanism. For shear-dispersed nanocomposites, there is little control over the orientation and alignment of the filler. Instead, alignment may be dictated by assembling a nanomaterial in the solid phase as a 'scaffold', before infiltrating the matrix material melt/precursor(s). The assembly may be created during synthesis (e.g. vertically aligned nanotube forests),[44-45] but most commonly, alignment is introduced in solutions where the nanomaterials are sufficiently mobile, before removing the solvent to form the solid aligned scaffold. The control over the alignment in

solution may be performed through laminar flow, at interfaces,[46] shearing of a concentrated solution,[47] external fields,[48] or use of liquid crystals.[41, 47, 49] Alignment may be introduced after composite formation, by applying shear to the nanocomposite, often when heated above the glass transition temperature to facilitate plastic motion of the filler. By controlling the interface of the filler, their dispersibility (both in the matrix and any initial solution processing steps) may be improved, allowing for the alignment to be improved via post-processing techniques.[50] The presence of nanomaterials in these processes may also concurrently aid the alignment of the polymer chains to improve load-bearing capacity of the matrix.[41] The improved and induced constituent alignments lead to anisotropic tensile stiffness and strength (improved if aligned in the loading direction), but can lead to dramatically reduced toughness's (Figure 5).[51] Through careful assembly and materials selection, both interfacial and dispersion effects may be balanced with improved alignment to increase strength while maintaining toughness, allowing for reasonable performance on both fronts.[50]

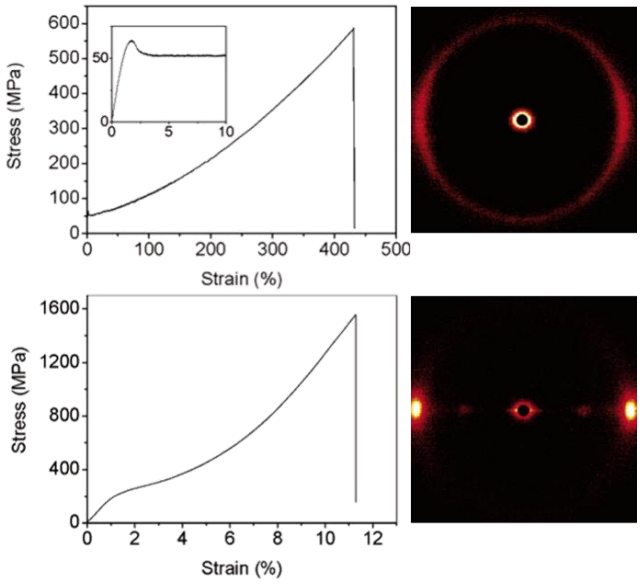

Figure 5. Mechanical Properties (left) and 2D X-ray diffraction of poly(vinyl alcohol)/carbon nanotube composite fibres before (top) and after (bottom) hot-drawing, showing dramatically higher strength (0.58 GPa to 1.6 GPa) and alignment but lower toughness (870 J g^{-1} to 50 J g^{-1}) after post-processing alignment. Adapted with permission from Miaudet *et al.*[51] Copyright 2005 American Chemical Society.

For 2D nanomaterials, alignment may be introduced in a laminar manner, for example through directional freeze drying, forming a porous scaffold for infiltration. Reduced graphene oxide (rGO) composites of this type[52] have been shown to increase crack toughness with low filler loading (2.9 MPa $m^{-1/2}$ at 1 wt.% loading). These laminar systems can be seen to be related to the "brick-and-mortar" systems described later

(Section 4.1), but with substantially lower filler loading fractions, which typically show higher work-to-fractures as they lack large matrix-rich regions.

3.1.3. Introducing Novel Failure Mechanisms

Alternative failure mechanisms are possible for conventional (nano)composites, through tuning of the overall structure hierarchy. The presence of nanofillers in simple nanocomposites toughens the bulk material through multiple mechanisms,[53] notably stress concentration suppression to delay damage initiation, damage diffusion via crack deflection, and filler debonding/pull-out. Nanofiller spatial distribution plays a critical role in the effectiveness of these mechanisms;[54] not only are agglomerates detrimental, but non-uniform distribution of non-aggregated fillers leads to inefficient reduction in stress concentrations.

Controlling the alignment of 1D nanomaterials can be used to modify mechanical behaviour of nanocomposites; highly aligned fillers increase uniaxial strength and stiffness, but for extremely high aspect ratio (10,000) 1D nanofillers, unaligned fillers may tangle into a network which deforms under stress,[55] allowing for improved toughening, especially when exfoliation is improved and promote entanglements. Furthermore, the number of tangles increases with strain, causing strain-hardening behaviour,[37] which dramatically increases toughness without sacrificing bulk strength or stiffness.

Nanofiller surface chemistry may be used to increase toughness, often introducing 'sacrificial bonds' (hydrogen bonds, π-π) between the fillers and the matrix. Many of these bonds may reform at different sites after the initial bonds are broken and the filler is partly pulled out, creating self-healing composites.[56] Sacrificial bond-forming moieties may be functionalised directly onto the filler to create an alternative approach to a matrix-free composite, as performed with cellulose nanocrystals reacted with ureido-pyrimidone-terminated polymers.[57] Sacrificial bonds may even be stored inside the filler; stacked-cup nanofibers[58] can be tightly bound to the matrix, leading to brittle failure of the external shell (Figure 6). The interior of the filler consists of π-π stacked coils of graphene which unravel upon crack propagation, dissipating large amounts of energy and increasing toughness by 112% (to 1.2 MPa $m^{1/2}$, 200 J m^{-2}) with the use of only 0.68 wt.% of nanofibers. Tough nanocomposites may also be created from multiple nanomaterial types with complimentary mechanical properties. For instance, CNT/graphene/poly (vinyl alcohol) fibres[59] deform with the reorientation of CNTs (towards the loading direction), which coupled to the high interfacial area of

graphene nanosheets, hinders crack propagation (deflection, blunting, etc.), creating fibres with the greatest specific toughness of any reported material to date (970 J g^{-1}, Figure 7).

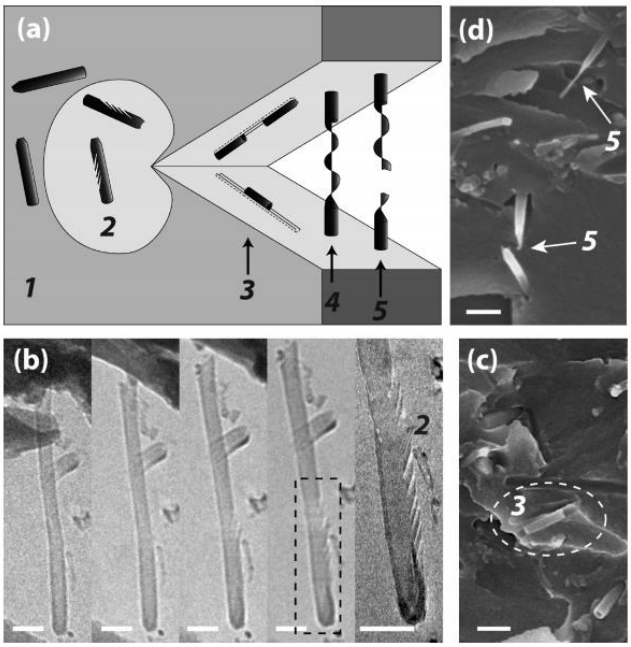

Figure 6. Stacked-cup nanocarbons with internal sacrificial bonds (a) schematic illustration of interaction between a propagating crack and Stacked-cup nanocarbons s in a polymer matrix (not to scale), (b) time-elapsed transmission electron microscopy micrographs of nanofiller under stress beginning to unravel, (c) nanocomposite fracture surface showing fragments of Stacked-cup nanocarbons , (d) nanocomposite fracture surface revealing ruptured nanofillers with dangling graphene sheets at ends due to unravelling. Scale bars are 100 nm in (b) and 200 nm in (c) and (d). Reproduced with permission from Palmeri *et al*.[58] Copyright 2010 American Chemical Society.

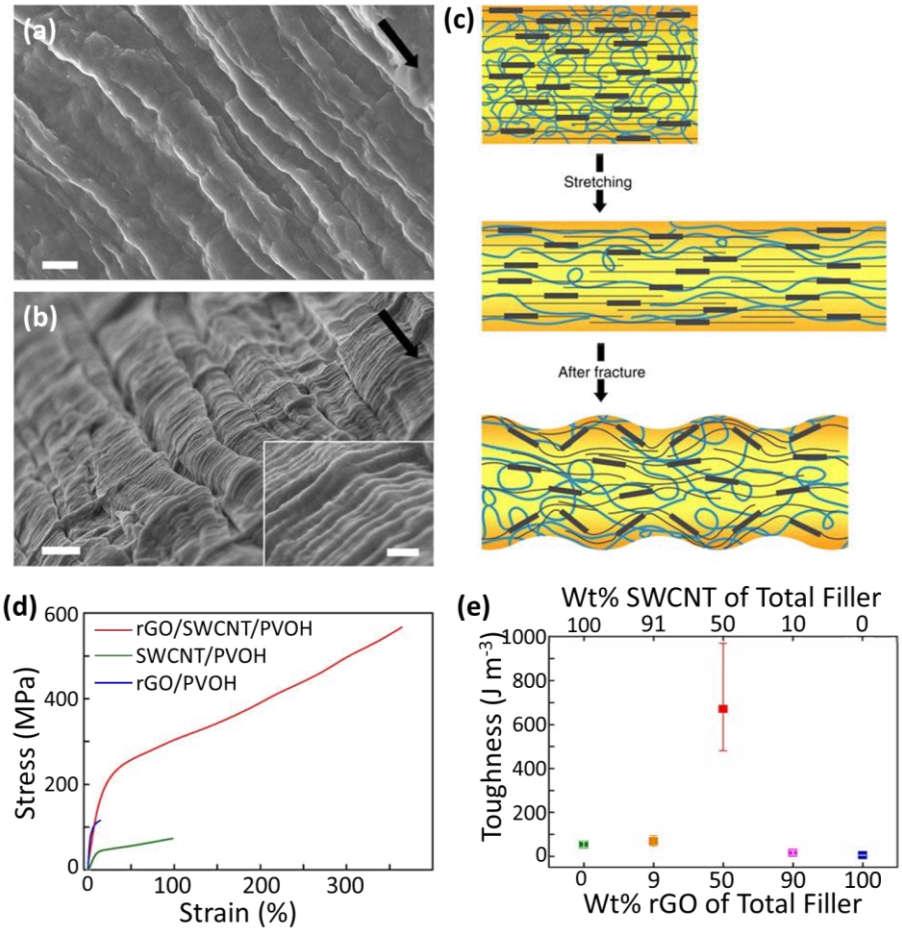

Figure 7. Poly(vinyl alcohol), SWCNT, rGO hybrid fibres (a,b) SEM micrographs before (a) and after (b) tensile testing. (c) Schematic of hybrid fibre containing rGO platelets (black rectangles), SWCNT bundles (black lines) and poly(vinyl alcohol) chains (blue lines) under tension and after fracture. (d) Stress–strain curves of hybrid (1:1 w/w rGO/SWCNT), SWNT, and rGO composite fibres. (e) Composite toughness (work-to-fracture) versus filler composition illustrating hybrid effect. Adapted from Shin *et al.*[59] licenced under CC-BY-NC-SA 3.0.

3.2. Toughening Fibre Reinforced Polymer Composites

The failure of high performance continuous FRP's are driven by the failure of the fibres, and the interface between the fibre-matrix. The interface strength in particular dictates the predominant deformation mechanism with strong interfaces (brittle fracture) and weak interfaces (pull-out) lead to differing behaviours in tension.[60] As such, control over the FRP toughness is most commonly performed at the interface (modifying shape, chemistry, or increasing interfacial-matrix volume) or dissipation of energy around the fibres e.g. through lay-up or hybridisation to reduce critical stress concentrations.[12] In tension, the matrix in continuous FRP composites does not provide significant contribution to the overall properties. However, in shear/compressive modes it provides a more significant effect; the matrix supports the fibres as they buckle

and fail forming kind-bands, rather than promoting delamination). The majority of modifications to continuous FRP composites are made to address this mismatch in shear properties between the fibre and matrix, to delay kink band formation through lateral support, or by the modulation[61] of adhesion between constituents. Other methods to control failure include predetermining the failure sites of FRP composites (weakening fibres[62]/interface[63]), which leads to increased fracture path and has been shown to increase toughness[64] at the expense of stiffness and strength.

Often, increasing toughness of a continuous FRP composite involves the introduction of (pseudo-)yield into the stress-strain response. A ductile response allows greater overall energy absorption by favouring damage accumulation over a larger area through multiple crack initiations and propagations. Approaches include the use of thin plies,[65] which increases the delamination stress[66] and, therefore, composite toughness, as well as the use of multiple fibre types for hybridisation. The hybrid approach (as recently reviewed by Swolfs *et al*.)[67] typically combines carbon fibres with a lower strength fibre such as glass fibres, and leads to higher toughness, both within and between plies, although results vary substantially between studies. The hybrid approach may be applied to discontinuous fibres, notably short carbon and glass fibres (millimetre length), which shows a pseudo-ductile response. The latter effect is actually more pronounced when the carbon fibres have been recycled.[68] The shape of the fibre itself can also be modulated to improve toughness; carbon fibres may be expanded locally through laser ablation/cutting to form an expanded region or "cotton-bud" ends,[69] respectively. Additionally, fibres can be coated intermittently along the length with beads of strongly adhering epoxy.[70] In both cases, the expanded regions anchor the fibre during pull-out, requiring large deformation of the matrix, dramatically increasing pull-out the toughness (Figure 8). While promising, altering the shape of the fibre has ramifications for packing efficiency and the current procedures are challenging to scale.

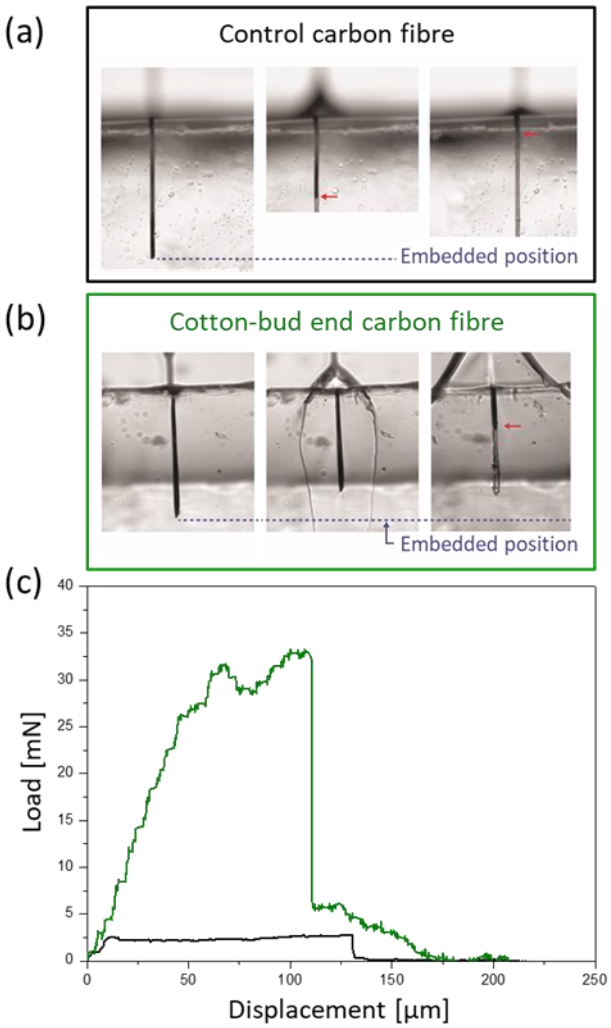

Figure 8. Optical micrograph series comparing the pull-out behaviour of (a) Control carbon fibre compared with (b) Cotton-bud end carbon fibre. (c) Load–displacement plots of the pull-out behaviour of fibres, work of pull-out 0.89 ± 0.19 µJ and 3.24 ± 1.22 µJ for control and cotton-bud end carbon fibre respectively. Modified with permission from Blaker *et al*.[69] Copyright 2016 American Chemical Society.

Modified FRP composites with nanomaterial fillers have been reviewed extensively.[71-73] In general, improving FRP composite toughness has been attempted through the introduction of nanofillers alongside the reinforcing micrometre scale fibres, at the fibre-matrix interface, and in the matrix. Nanofiller addition is most easily integrated into current FRP manufacture in the interlaminar region, as the viscosity of the matrix is unaltered, preventing delamination, and improving interply fracture toughness. The nanofillers, which may be included, include discrete nanoparticles (such as carbon nanotubes,[74] graphene nanoplatelets,[75] 2D nanoclays[76]) or continuous nanofillers such as electrospun nanofibers[77] or CNT forests.[78] Regardless of approach, it is critical that the interply spacing remains unchanged as thicker matrix regions between the plies can lead to misinterpreted toughened response.[79] Additionally, intraply modifications to create the

hierarchical integration of nanomaterials into FRPs is possible, creating so-called multiscale composites. Homogenous distribution of nanomaterials throughout the matrix may toughen FRPs, with the nanofillers redistributing stress concentrations,[53] deflecting cracks,[80] and introducing nanofiller pull-out;[53] however, as with simple nanocomposites, effective dispersion at high loading remains challenging.[81]

Alternatively, the nanofillers can be limited to the FRP fibre/matrix interface as the onset of mechanical damage often occurs in this region and assembly on the fibres before matrix infiltration avoids the difficulties of matrix-dispersion, while facilitating high (local) filler loadings. Several assembly routes are known, including direct nanomaterial growth on the fibre surface,[82] dip-coating,[83] and adhesion with covalent[84] or ionic bonding.[85] Nanofillers increase bulk FRP composite toughness via nanoscale toughening mechanisms, in addition to mesoscale toughening enabling plastic deformation of the filler/matrix interface through mechanical interlocking. Care must be taken to avoid damaging the fibre during deposition[86] (particularly if nanofillers are grown directly on the fibre),[87] and forming agglomerates, which lead to high local stress concentrations.

While stiff 1D,[87] 2D,[84] or 0D[85] nanofillers may be introduced at the primary reinforcement fillers/matrix interface, 1D materials are most common, as 0D nanoparticles provide only modest improvement, while 2D nanoplatelets often suffer from fibre curvature coinciding with the filler lateral length scale.[88] As such, high nanosheet aspect ratios do not allow for a conformal or organised layered assembly about the fibre circumference, so aspect ratios must be significantly reduced to avoid forming agglomerates. Introducing nanofillers at the primary fillers/matrix interface may be coupled to introducing dilute nanofiller into the bulk matrix (1 wt.% CNTs), with the resultant FRP mechanical properties exceeding either strategy in isolation.[89] High toughness “brick-and-mortar” nanocomposites (see Section 4.1) can be introduced as a layer at FRP/matrix interfaces,[82, 90] using scaled-down nanoreinforcements to fit fibre curvature.

4. Tough Nanomaterial Architectures

In contrast to classic composites, mixing nanomaterial fillers into a homogenous matrix as a nanocomposite, or integrating into a FRP composite, nanomaterials may be assembled into bulk materials in the absence of a continuous matrix. Without a matrix allowing for stress transfer, the constituent nanomaterials must either transfer load directly to one another or through an intermediary local species, so careful assembly of the material architecture is paramount. However, in theory, this approach allows for the

design of materials with up to 100% volume fraction high performance nanomaterial, leading to high strength, stiffness, and toughness.

4.1. Brick & Mortar Assemblies

Nacre is a natural material found inside mollusc shells formed of a layered composite in a so-called "brick-and-mortar" (B&M) structure.[91] Nacre consists of intrinsically mediocre materials; 95 vol.% of stiff and brittle aragonite platelets embedded in 5 vol.% of soft chitin-containing organic framework. The complex hierarchical structure of nacre enables multiple toughening mechanisms to operate across the entire range of length scales,[92] exhibiting a highly desirable combination of high strength and high toughness.[93] At the nanoscale, nacre consists of one-dimensional nanofibrillar chitin alongside aragonite nanograins (≈ 30 nm) glued together with a biopolymer to form 200-900 nm thick and 5-8 μm wide aragonite platelets[94] with nano-rough "asperities" on the surface.[95] At the micrometre length scale, the aragonite platelets appear interconnected through the organic framework via mineral bridges.[96]

Nacre's high strength derives from the high proportion of rigid platelets, yet nacre's toughness is about three order of magnitude higher than pure aragonite.[93] The platelet aspect ratio is sufficiently low to prevent platelet fracture;[97] instead material fracture occurs through B&M interfacial failure and platelet pull-out. The structure undergoes multiple deformation mechanisms during pull-out, dissipating a substantial amount of energy,[92] including platelet jamming upon sliding, shear resistance from nanoasperities, breaking of mineral bridges, nanograin rotation, and organic framework viscoelastic deformation. Various features of nacre also contribute to deflecting, bridging, and blunting propagating cracks, amplifying energy absorption as compared to failing via a singular straight crack.[98] In short, the complex hierarchical arrangement, abundance of filler/matrix interfacial interactions, and synergy between components provide nacre with outstanding mechanical properties.

It has been predicted that the performance of nacre-inspired structures could be improved by decreasing the size of the inorganic platelets while retaining phase proportions, geometry, and aspect ratio.[99] Because the toughness of nacre emerges from interface deformation, increasing the interface volume fraction to the matrix through decreasing platelet dimensions should amplify toughness.[100] The B&M structure of nacre has inspired many researchers to develop layered nanomaterial composites for strong and tough bulk materials (Figure 9).[101] The term "brick-and-mortar" is preferred here to describe the synthetic nanocomposites in lieu of

"nacre-mimetic" or "nacre-like", due to the substantial difference in platelet aspect ratio, phase proportions, and length scales of the constituent materials.

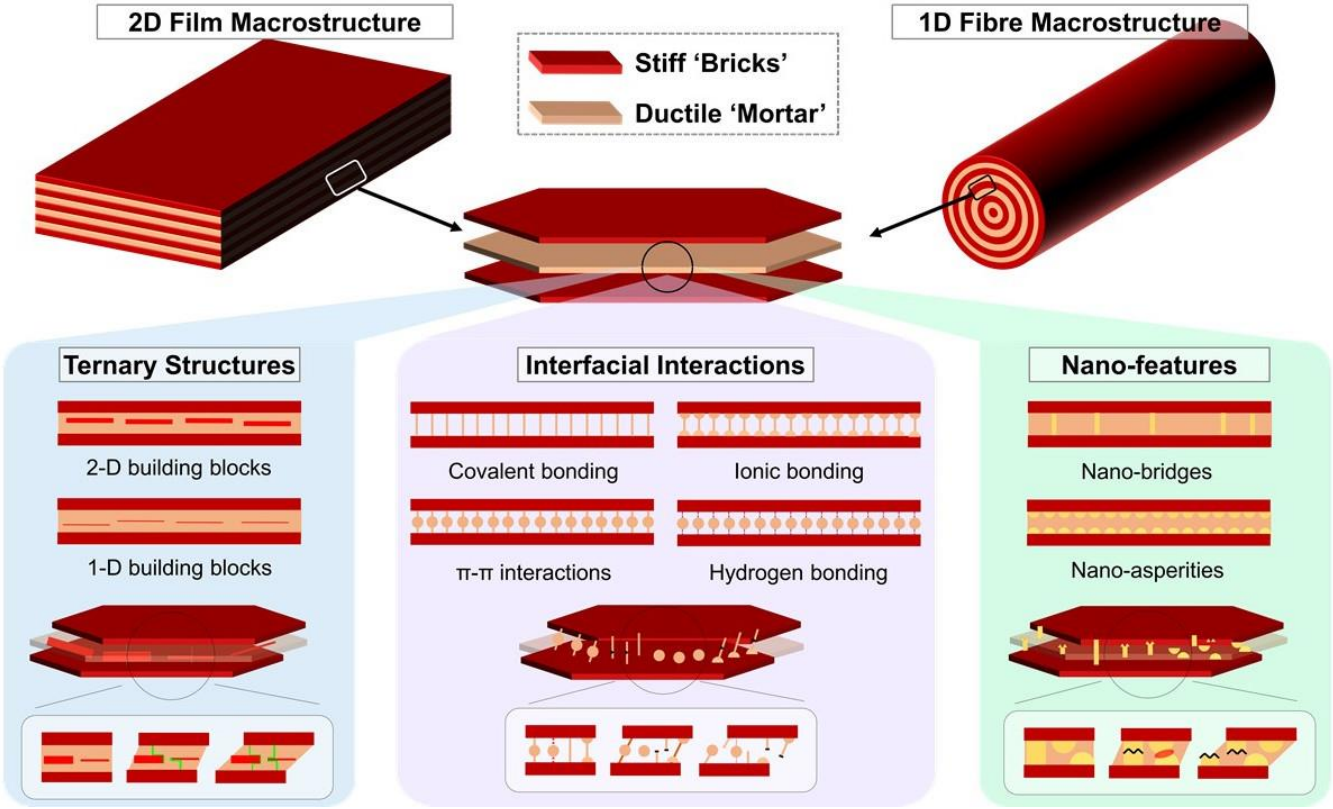

Figure 9. Hierarchical structure of "brick-and-mortar" assemblies, and interlaminar modification routes; ternary structures (addition of a second type of nanoreinforcements), interfacial bonding between bricks and mortar, and nanofeatures linking bricks during platelet sliding. Bottom: schematic representation of the different interfacial deformation mechanisms with increasing shear, from left to right.

A broad range of methods have been used to develop B&M architectures, including layer-by-layer assembly,[97, 102] vacuum filtration,[35, 103] solution-casting,[104-105] vacuum evaporation,[59, 106] and freeze-casting.[107] Creating scaled-down B&M nanostructures while retaining phase proportions, reinforcement aspect ratio, and packing geometry found in nacre is non-trivial; nevertheless, the B&M arrangement of natural nacre has been scaled-down by over one order of magnitude while retaining the aforementioned characteristics.[108] Strong electrostatic interactions between the layers combined with the high proportion of inorganic phase (≈ 90 wt.%) produced a stiff and strong material, replicating some toughening mechanisms of nacre such as crack deflection and platelet sliding/interlocking. When 'bricks' are further minimised to nanometre thicknesses (most commonly using montmorillonite clay mineral,[102, 104, 109] and graphene/graphene oxide (GO) nanosheets),[103] approaching the thickness of the 'mortar', ideally dispersed nanosheets represent less than 50

vol.% of the overall nanocomposite, far from nacre's 95 vol.%. The incorporation of GO at ≥70 wt.% causes significant waviness and stacking, limiting GO/matrix interfacial interactions,[110] while montmorillonite nanosheets form tactoids at >70 wt.%, compromising the mechanical properties;[111] as such, lower loadings are used in spite of the loss of potential stiffness and strength. However, the use of high performance nanosheets with abundant oxygen-containing functional groups, such as GO, allows for the engineering of strong and complex filler/matrix interfaces.

The incorporation of covalent or/and non-covalent bonding in the B&M nanocomposite allows tuning of strength, toughness, and fatigue behaviour. For non-covalent interactions, ionic bonds can significantly improve the mechanical properties of synthetic nanocomposites; metal ion-based strategies,[112] ionically bonding the nanoreinforcements, improve strength (+24.1 – 70.8%) and toughness (+18.6 – 110.1%). However, non-covalent bonding can also be easily compromised in solution, due to salt and pH interferance.[113] Hydrogen bonding[114] and π-π bonds[115] also increase strength, yet as relatively weak interactions, they remain the most easily broken component, allowing for crack deflection and plastic deformation.[103] Multiple filler/matrix interfacial interactions may be present simultaneously,[115] e.g. with staged failure of hydrogen and π-π bonding, and subsequent polymer deformation (extension, uncoiling and rupture) in parallel with nanosheet pull-out to increases toughness concurrently (15.3 MJ m^{-3}).

Conversely, strong covalent bonding can also be incorporated to cross-link platelets to the mortar, by use of linear molecules, branched polymers or 3D network resins; long molecules being preferable over short molecules as they undergo larger deformations.[106] Similarly to FRPs, strong filler/matrix interfacial interactions lead to efficient stress transfer high strength, and retained structural integrity of B&M nanocomposites, but trigger limited toughness.[103] Covalent bonding may be combined with alternative strategies synergistically, namely ionic bonding,[116] improving strength (400 MPa) and toughness (20 MJ m^{-3}) to values higher than that of natural nacre. Similarly, combining covalent and weaker non-covalent bonding[35, 115-117] provide, to date, among the greatest strength (300- 500 MPa) and toughness (2-20 MJ m^{-3}) in B&M systems.

Beyond the B&M layered architecture of nacre (and associated interfacial interactions), nacre's mechanical properties are influenced by 1-dimensional nano-fibrillar chitin, which acts synergistically with the 2D aragonite platelets.[93, 118] Inspired by this hierarchy, primary nanosheet reinforcements have been combined with additional (1D[42, 119-120] or 2D[36, 103, 121]) reinforcements to form ternary nanocomposites, with the coaction of multiple reinforcing blocks improving mechanical performance. In general, the 2D component is best suited

to deflecting and arresting cracks, while the 1D filler bridges cracks. For example, when distributed evenly at the interface between the 2D nanosheets and the soft polymer, 1D nanofibular cellulose can bridge propagating cracks, while also promoting further resistance to nanosheet sliding.[42] CNTs have been shown to be capable of preforming the same role, and when introduced to hydrogen-bond-reinforced B&M systems, the combination of hydrogen bond cleavage alongside 1D pull-out after nanosheet sliding increases the amount of energy dissipated during fracture.[119] 2D reinforcements may also be used as secondary reinforcing blocks, (e.g. amorphous alumina nanosheets) improving long-range crack deflection to further increase toughness.[103] More recently, a ternary B&M nanocomposite consisting of two polymers and one nanosheet has been designed;[122] the nanocomposite benefits from extensive hydrogen bonding, with increased toughness (27.5 MJ m^{-3}), but exhibits relatively low strength (50 MPa) due to the limited proportion of reinforcing nanosheets.

The mechanical properties of these synthetic B&M nanocomposites could be further improved by implementing the multiscale deformation mechanisms observed in nacre. Nanoasperities on the surface of nacre's aragonite platelets increase resistance to platelet sliding, and can be mimicked by forming platelets with roughened surfaces.[123] Approaches have included biomineralisation on platelet surfaces,[123] and bidirectional freezing trapping inorganic particles by the growing ice,[107] with nanocomposites exhibiting strain-hardening from the roughened surface increasing sliding resistance. Directional freezing can also form inter-lamellar bridges between bricks,[107] which may act akin to natural nacre mineral bridges, expanding crack extension. However, they are infrequently formed and randomly distributed throughout the nanocomposite.

Recently, a so-called 'inverse-nacre' has been developed, with layers of flexible polymer platelets embedded in a 'mortar' network of rigid nanofibers.[124] The classic nacre-like deformation behaviour was observed in the material, with fibres at the platelet interface dissipating stress through mutual sliding, crack deflection, and crack bridging, with absolute strength (40 MPa) and toughness (4 MJ m^{-3}) currently lower than conventional B&M approaches.

Most commonly, B&M assemblies form planar 2D macrostructures (i.e. films and coatings), but 1D macrostructures may also be assembled into fibres tens of microns in diameter,[114, 125-126] using wet-spinning, with liquid-crystal dopes available at high fillers concentrations to improve axial alignment.[125] At the nanometre length scale, fibres exhibit a layered nanostructure similar to planar B&M nanocomposites, but with additional radial geometry. By combining wet spinning and dip-coating, the synergistic effect arising from multiple interfacial filler/matrix interactions observed in planar nanocomposites may also be applied in B&M

fibres. Covalent bonds in tandem with ionic bonds restrict nanosheet sliding/pulling-out, leading to high strength (842 MPa) and high toughness (16 MJ m^{-3}).[127] GO-based B&M fibres with high polymer content (~70 wt.%) have been twisted to form a spring-like coil providing macroscopic hidden length.[128] At the micrometre length scale, twisted fibres exhibit a smooth helical macrostructure, with a uniform layered nanoscale structure. While exhibiting low strength (300 MPa) compared to other high-performance fibres, the untwisting of the fibre in tension enables a very high strain-to-failure (300%), facilitating remarkable toughness (460 MJ/m^3).

In addition to their high mechanical performance making them ideal candidates for load-bearing applications, B&M materials are suitable for (multi)functional applications including flexible gas barriers,[104, 122] fire-retardants[36] and conductive materials.[128] Graphene B&M systems also facilitate electronic applications with high mechanical performance (as summarised in previous reviews),[101, 129-130] including transparent electrode for organic photovoltaics, strain sensors, supercapacitors, actuators, nanogenerators, filters and electromagnetic interference shielding.

4.2. Pure Nanomaterial Papers

Uncontrolled assembly of high aspect ratio (1D/2D) nanomaterials leads to randomly orientated "papers", usually with poor mechanical properties, regardless of the intrinsic performance of the nanoparticles (e.g. CNT 'buckypapers').[131] Cross-linking of these papers with strong ionic[132] or covalent[123] bonds mildly improves stiffness and strength, but the assemblies become brittle and toughness is reduced. Aligned 2D macrostructures may be formed (e.g. through flattening of vertical arrays, or magnetic field alignment) to improve uniaxial performance. However, limited stress transfer leads to performance inferior to that of B&M assemblies and standard nanocomposites. These approaches are often used to create scaffolds for matrix infiltration (composite manufacture),[44] which suffer from agglomeration issues and do not adhere to the RoM.[131]

Ironically, the main exception for pure nanomaterial papers are, akin to regular paper, made of cellulose and not the ultrahigh strength nanomaterials. Unlike the weak vdW interactions between most nanomaterials, the hydroxyl-rich surface of cellulose facilitates hydrogen bonding between adjacent nanomaterials providing higher inter-material bonding than intrinsically stronger nanomaterials such as CNTs. Papers may be made from any of the length-scale cellulose materials, and decreasing constituent size leads to increasing paper

strength,[133] as is expected from the Griffith criterion. However, in contrast to typical systems, as constituent size decreases, toughness also increases. This increase is attributed to the reformable hydrogen bonding between sliding adjacent fibrils, with smaller species containing more interfibril bonds due to the increased surface area.[133] Resultantly, pure nanocellulose papers can simultaneously demonstrate reasonably high toughness (7.3 MJ m^{-3}) and strength (235 MPa) even for randomly aligned papers.[134] Through the use of high molecular weight, high intrinsic order cellulose, and by introducing alignment and densification in the paper via wet-drawing and compression,[135] respectively, the degree of inter-fibril interactions may be increased, leading to very high toughness (25 MJ m^{-3}) and strength (1 GPa) concurrently (Figure 10).

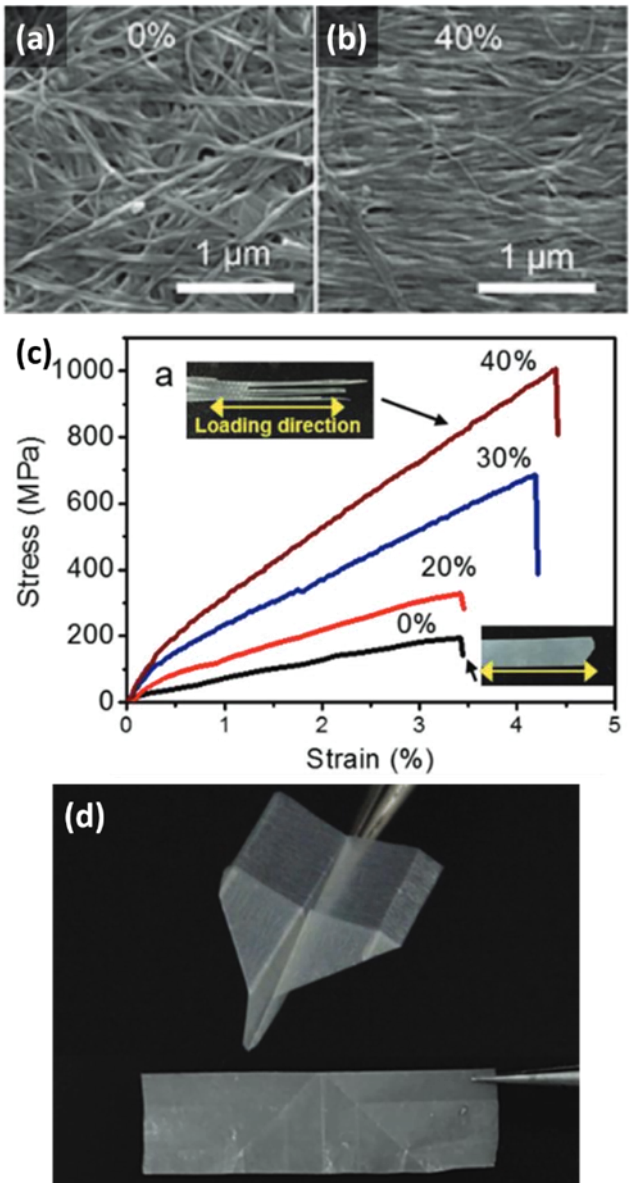

Figure 10. Cellulose nanocrystal paper from *Acetobacter xylinum* bacteria aligned through wet-drawing. (a) scanning electron microscope (SEM) micrographs of as-grown cellulose film; (b) SEM micrograph of film after wet drawing to 40% strain; (c) tensile stress-strain curves of cellulose nanocrystal paper wet-drawn to varying

degrees; (d) digital photographs of cellulose nanocrystal paper aeroplane being folded and unfolded to illustrate its non-brittle, tough nature. Adapted with permission from Wang *et al.*[135] Copyright 2018 John Wiley and Sons.

4.3. 1D Nanomaterial Yarns

Pure high aspect ratio nanoparticles may also be assembled into 1D macrostructures, i.e. fibres, often called "yarns". Most commonly, these materials are axially aligned 1D nanomaterials including boron nitride nanotubes[136] and cellulose nanofibrils,[137] but most interest has revolved around CNTs.[138] There are mainly three yarn assembly routes: coagulation of a nanofiller dispersion, twisting of (typically CVD-grown) aerogels, and manipulating as-grown 2D arrays; these assembly routes have been reviewed for CNTs,[139] but are largely applicable to all high aspect ratio nanomaterials. Given the often-irregular cross-sectional area of yarns, strength/stiffness should be given as a function of linear mass density (GPa $SG^{-1} \equiv$ N tex^{-1}). Yarns have shown specific strength[140] (3.5 N tex^{-1}) and stiffness[140] (200 N tex^{-1}) approaching that of carbon fibres, but at significantly higher toughness[141] (107 J g^{-1} = 171.2 MJ m^{-3} assuming 1.6 g cm^{-3}), making them ideal replacements for next generation high toughness FRP composites.

The key to high axial performance yarns is their architecture (Figure 11) – CNT yarns do not consist of a singular array of end-to-end aligned nanotubes, but instead, of a hierarchy of bundles. Locally, tens of CNTs form small compact bundles held together by π-π interactions with very high intrinsic toughness[141] (~500 J g^{-1}) from the maximised inter-CNT contact area, with longer bundles having greater total intra-bundle interactions and providing higher yarn strength.[142] Bundles do not have a perfect structure or alignment/orientation, instead, partially bundled nanotubes at the edges fray, and may entangle with, or be incorporated into, adjacent bundles, facilitating stress transfer across the entire structure. At the micrometre length scale, bundles may tangle, leading to a dramatic decrease in net CNT alignment. At the macro-scale, the structure can be predominantly aligned axially, or twisted helically as a result of synthesis methodology or post-processing (*vide infra*). Under tension, exterior CNTs initially carry the applied load, with the inter-bundle-penetrating CNTs and direct bundle-bundle contact transferring stress into the yarn interior.[143] The high toughness of these yarns is ensured by the presence of a yielding behaviour, typically at 1 – 2 % strain, after which bundles first realign axially,[141] with inter-bundle nanotubes straightening, followed by both inter- and

intra-bundle slippage. The slippages create additional bundle-entanglements and subsequently, yarns undergo strain-hardening deformation before failure through pull-out, leading to high total energy absorption.

Analogous to composite materials, the degree of alignment of the constituent materials along the yarn axis has a significant impact on the mechanical performance.[144] High alignment improves the stiffness and strength of the yarn, while poor alignment is coupled to greater entanglement and facilitates reorientation of hidden length, increasing the ultimate strain-to-failure (up to ~15%). However, deliberately decreasing alignment does not improve toughness, as gain in strain-to-failure is offset by a significant reduction in strength.

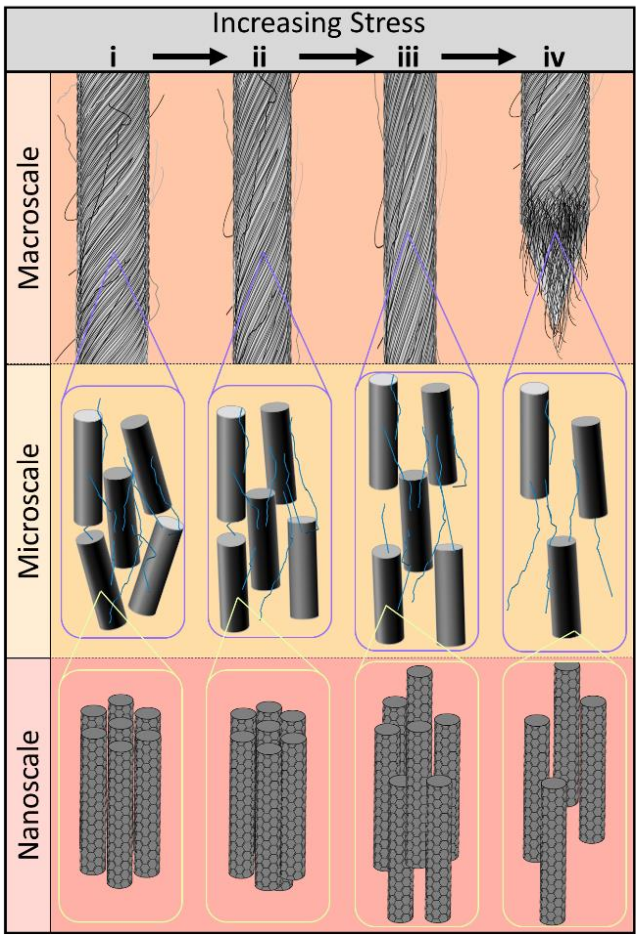

Figure 11. CNT yarn structure with increasing tensile stress. (i) Unstressed yarn with macrostructure of helically twisted yarn containing frayed bundles on the surface, microstructure of partially aligned bundles connected by inter-bundle contacts and interconnecting frayed nanotubes, and nanostructure of co-aligned hexagonally packed individual CNTs; (ii) When stressed, bundles reorient along yarn axis at the microscale, decreasing yarn diameter as macroscale-twist tightens; (iii) interbundle (microscale) and intrabundle (nanoscale) slippage occur; (iv) fibre fails through bundle and CNT pull-out.

In spite of noticeable intrinsic changes in filler/matrix interface area and strength, the number of walls and crystallinity of CNTs has a surprisingly minor impact on the mechanical performance of the yarn.[144-146] The aspect ratio of CNTs clearly dominates the properties of the material;[146] ends can act as defects and carry less load,[147] and longer CNTs contain fewer ends per yarn. Longer CNTs are also more prone to penetrating and entangling with multiple bundles; in extreme cases, they may form bundles spreading across the entire yarn circumference, carrying load without inter-bundle stress transfer. It is predicted that by using CNTs with an aspect ratio of 100,000, the yarn strength could match that of individual CNTs (30 GPa).[146]

The hierarchy of the yarn is controlled by a range of pre-synthesis (e.g. self-alignment from liquid crystal precursors), *in situ* (precursor dilution),[144] and post-synthetic (drawing, twisting, densification) processes. Twisting the yarn under tension is most common, increasing density and organisation;[138] densification may also be performed under pressure, such as flattening to form a ribbon.[148] Although the load-bearing capability (N tex^{-1}) and, therefore, the specific toughness (J g^{-1}) of denser yarns does not increase, the reduced cross-section leads to higher strength/stiffness (N m^{-2}) and toughness (J m^{-3}).

For aerogel-spun CNT yarns, a co-synthesised coating of organic "polymer"[141] (5 – 15 wt.%) is incorporated between nanotubes. The coating improves inter-bundle stress-transfer, while further crosslinking of the organic material[140] delays bundle-sliding without altering the nanotubes, increasing strength, stiffness, strain-to-failure, and toughness. Akin to the unaligned papers, yarns may also be used as scaffolds[142, 145] for thermoplastic infiltration, forming composites. While the filler network continues to carry the load – stiffness remains constant[142] – both toughness and strength improve slightly (~10%) as a result of the increased inter-bundle stress transfer.

Cellulose is an ideal material for yarns; the hierarchical structure of wood intrinsically contains cellulose yarn-like fibres (of nanocrystals/fibrils wound and linked with lignin) of high intrinsic strength.[149] These natural fibres may be isolated (e.g. paper making) and the strength of the strongest individual fibres (1.5 ± 0.41 GPa, unbleached softwood[150]) remains unsurpassed by synthetic cellulose yarns or composites to date. Advances have been made in improving toughness of cellulose-based yarns, such as those spun from cellulose nanofibrils,[151] which show the same deformation mechanics seen in papers (Section 4.2). The synthetic fibres increase in strength and stiffness with increasing cellulose fibril length, while the strain-to-failure also slightly increases, leading to a significant amplification in toughness, from ~27 MJ m^{-3} to ~48 MJ m^{-3} (measured from provided stress-strain curve[151]). However, the behaviour is dependent on water in the structure acting as a

plasticiser, leading to diminished toughness at low humidity (Figure 12b). Crosslinking the cellulose nanofibrils within the yarn leads to a significant increase in strength, but a loss of the ductile yielding behaviour and a reduction in toughness (Figure 12c). The highest toughness cellulose yarn to date comes from functionalisation of cellulose nanocrystals with spider silk proteins.[152] The functionalised protein increase inter-fibril stress transfer and, therefore, strength (from 830 MPa to 1 GPa) and additionally, the proteins unfold under tension, maintaining stress transfer during fibril-sliding, and increasing strain-to-failure (6% to 10%). The latter achieved a cellulose nanocrystal toughness record of 55 MJ m^{-3}.

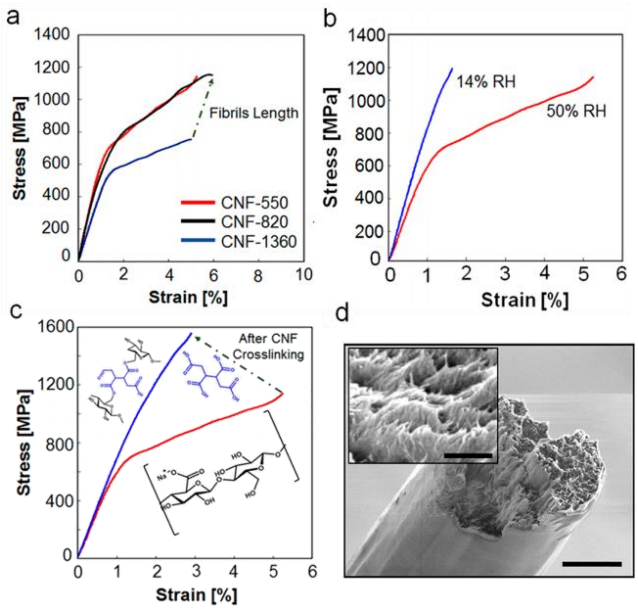

Figure 12. Tensile mechanical properties and nanostructure characterization of cellulose nanofibril yarns. (a) Behaviour of yarns made of cellulose nanofibrils of increasing length in order blue < black < red. (b) Tensile behaviour of yarns in varying relative humidity. (c) Behaviour of yarns before and after crosslinking. (d) SEM micrograph of yarn failure cross section, scale bars 3 µm and 400 nm (inset). Reproduced with permission from Mittal *et al.*[151] licenced under CC-BY.

2D nanomaterials may also be used for yarn synthesis, such as liquid crystal dopes of GO wet-spun into yarns. However, mechanical properties, including toughness and strength, are noticeably lower than their 1D nanomaterial counterparts, likely due to the absence of the hierarchical bundle architecture. GO yarn strength may be enhanced by introducing cations, forming inter-sheet ionic bonding via oxygen containing groups[153] (strength and stiffness of 365 MPa and 6.3 GPa, respectively) or by flattening densification.[43] Chemical reduction[153] or thermal graphitization[34] of GO to graphene yarns dramatically increases mechanical properties due to the significantly higher stiffness of graphene over GO – thermal reduction may also introduce covalent cross-linking to strengthen (and embrittle) yarns. The architecture may be better controlled by concurrent use

of large and small GO flakes,[34] providing a more compacted and ordered post-reduction structure with strength (1.1 GPa) and stiffness (130 GPa) approaching those of CNT yarns, but at lower toughness (~7 MJ m^{-3}, as measured manually from provided stress strain) due to the low strain-to-failure and brittle failure.

The most obvious route to application for high strength, high stiffness, tough yarns (or nanocomposite fibres, Section 3.2) is as replacement for continuous fibres in FRCs. However, several significant hurdles require addressing prior to widespread application, notably composite integration and scalability. For integration, the use of yarns in a brittle matrix, such as epoxy, will likely not lead to a significant increase in toughness and risks yarn infiltration, producing brittle, low toughness fillers. Tougher matrices are likely required which may prevent full exploitation of the inherent stiffness/strength of the yarns. Relatedly, the interface must be highly tuned to facilitate sufficient shear transfer, which will require yarn-dependant surface chemistries to be developed. Until these issues have been addressed sufficiently, caution is required when directly comparing the properties of a yarn to existing composite structures, or indeed to the existing reinforcing fibres which have established integrations. Secondly, the scalability of yarns has yet to be demonstrated at pilot plant scale, particularly through CVD aerogel synthesis. While coagulation fibre spinning is fundamentally scalable and may take advantage of existing polymer fibre spinning infrastructure, the properties are often inferior to the CVD materials which are more challenging to scale.

4.4. 0D Nanoparticle Assemblies and Supracrystals

Low aspect ratio (0D) nanoparticles usually form weak assemblies, unless carefully assembled with interposing ligands (forming supracrystals, *vide infra*), with a few notable exceptions. 'Octopod' CdS nanocrystals may assemble into interlocked-chains, which subsequently link to form an intrinsically porous 3D macrostructure exhibiting high stiffness (8 GPa)[154] and highly plastic deformation (Figure 13), although toughness had not to date been quantified. Alternatively, fullerenes – commonly C_{60} – are synthesised as powders of body-centred cubic crystals, but under high pressure and temperature (generally >10 GPa and >500 °C) form ultra-hard fullerite. The structure and mechanical properties vary notably with synthesis conditions,[155] while crosslinking between individual fullerenes (at more extreme conditions, the fullerenes convert to 'aggregated diamond nanorods')[156] form a macrostructure with remarkably high stiffness[157] (450 – 850 GPa) and among the highest hardness[157] ever measured (310 GPa). Like the other properties, the fracture

toughness is highly variant with synthetic conditions, typically[158] around 7-10 MPa $m^{-1/2}$ although values of ~20 MPa $m^{-1/2}$ have been reported.[155]

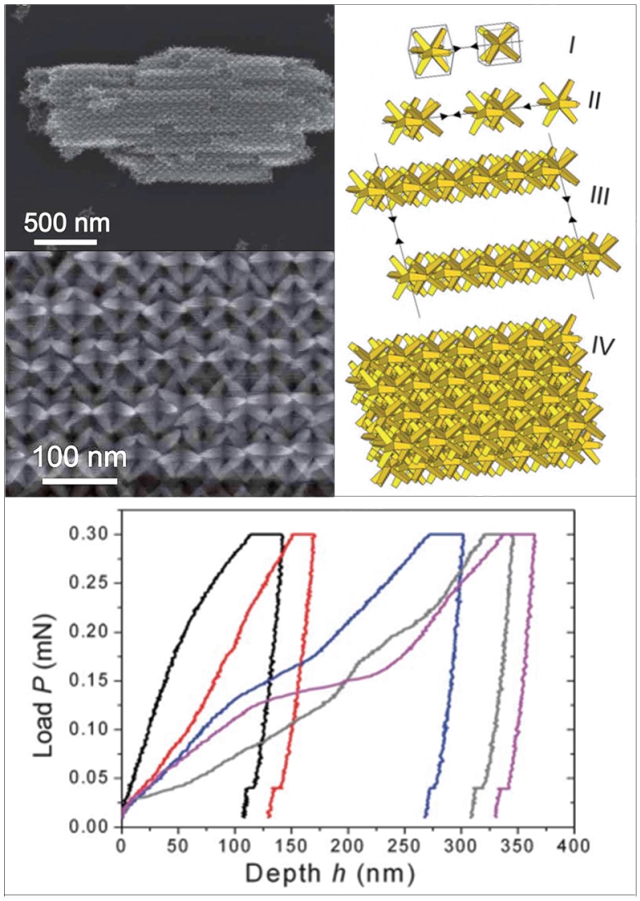

Figure 13. Octapod CdSe/CdS nanoparticle assembly. Top left) SEM micrographs of assembly. Top Right) Schematic of assembly process; Bottom) Compressive load-displacement measurements to differing depths. Reproduced with permission from Ceseracciu *et al*.[154] Copyright 2009 Royal Society of Chemistry.

Nanoparticles (NP) are highly ordered at the atomic scale, but often assemble into amorphous structures in the solid state which contain a high concentration of defects, leading to premature fracture at low stress and low toughness. However, so-called supracrystals may be formed from assembling NP 'cores' into superlattices at the meso/nanoscale; assembly processes were recently reviewed.[159] Supracrystals are predominantly created for their unique optical, electronic, photonic, and magnetic properties, but also exhibit a range of interesting mechanical behaviours as a result of their well-defined arrangement. The cores may scale from 1 to 100 nm, and must be well-solvated and individualised in solution before assembly to avoid amorphous, unordered products.[159] Most commonly, cores are inorganic or metal lattices, although covalent nanospecies[160] and polymers[161] may be used. Inorganic/metallic NPs require ligands to limit sintering, aid

solubility, and can be carefully selected/modified to tune the mechanical properties of the bulk supracrystal. The NP loading fraction of supracrystals is dictated by the NP surface area/volume ratio and ligand length/coverage efficiency. To date, solution-grown supracrystals only exhibit sub-millimetre diameters. The superlattice packing of the supracrystal is predominantly dominated by constituent NP shape with typically unary (quasi-)spherical NPs, usually driven by packing efficiency, forming close-packed lattices (hexagonal close-packed, and face-centred cubic). Supracrystals differ from simple nanocomposites in several key manners: firstly, supracrystals do not possess any continuous matrix phase in which the stresses are transferred, implying that deformation only occurs when direct forces are applied to the fillers. Secondly, while nanocomposites mechanical behaviour is drastically limited by voids and matrix-rich regions (from agglomerations and poor dispersion), supracrystals are perfectly dispersed and agglomerate-free despite their high loading fractions.

The absolute mechanical properties of supracrystals vary significantly with constituent materials and assembly. However, high strength[162] (630 MPa), stiffness (19.5 GPa),[163] hardness (18 GPa)[164] with varying deformation behaviours have been achieved, via tuning of (supra)crystallinity, ligand chemistry, core material, and macrostructure. As-grown supracrystals typically show viscoplastic behaviour from core displacement[165] and follow the RoM; high stiffness and hardness are expected from the high core volume fraction, with stiffness falling between the constituent materials intrinsic stiffness values.[163]

The size of the NP core impacts the mechanical performance of the supracrystal, although trends can reverse depending on systems. While larger stiff cores improve stiffness and hardness,[166] via an increase filler volume fraction, they may also reduce the packing efficiency and order and, therefore, have a detrimental impact on the mechanical performance of the supracrystal.[167-168] The intrinsic crystallinity of the cores themselves can dictate supracrystal performance, with monocrystalline cores both assembling into supracrystals faster, and exhibiting greater stiffness than polycrystalline,[169] amorphous,[170] or multiply-twinned NPs.[169] The change in modulus may be attributable either to lower intrinsic stiffness of the polycrystalline cores, or the reduction in superlattice order versus monodomain NPs. While non-spherical cores are also commonly employed for superlattice formation, their mechanical properties have not been investigated to date.

In supracrystals, the interparticle bonding, which controls the stress transfer capability and deformation mechanisms of the material, depends on both ligand-NP bonding and inter-ligand bonding. To maximise

mechanical properties, the core/ligand ratio must be tuned correctly to facilitate full core coverage, with both insufficient[165] and excess free ligand[166] deteriorating bulk properties. Hence, it is important to carefully wash free excess ligand from the nanoparticles after synthesis and prior to supracrystal assembly. Ligand-NP bonds are necessarily strong to prevent dehesion of ligand from the core in solution, and are selected based on the core chemistry (e.g. thiols for gold cores,[168] and carboxylates/phosphinates[165] for metal oxide cores), but there is much greater flexibility in inter-ligand bonding (Figure 14). Simple vdW-dominated systems (particularly alkyl chains) are most common, with longer chains increasing the per-ligand interaction forces.[170] However, the weak nature of these interactions lead to a highly brittle material with low toughness,[171] often on the order of 40 kPa $m^{-1/2}$. Inter-ligand vdW interactions may also be increased further through interdigitation[172] by ensuring full coverage of monodispersed ligands; non-packed ligands can bend towards its adhered core, limiting inter-digitation. At polymeric ligand lengths, while the stiffness and hardness plateau,[173] fracture toughness continues to rise as interpolymer entanglements increase, introducing craze formations during fracture. At intermediate polymeric ligand lengths, the supracrystal toughness is higher than the polymer of the same M_w as the polymer in the supracrystal are pinned to the NP, restricting deformation motions, stabilising crazes and resisting crack propagation. The effect leads to the toughness matching the toughness of high molecular weight polymers (which by virtue of increased molecular length also shows heightened connectivity and craze stabilisation) at a lower threshold.[173] It is noted that the crack toughness of the NP-free homopolymer is not exceeded by the supracrystal.

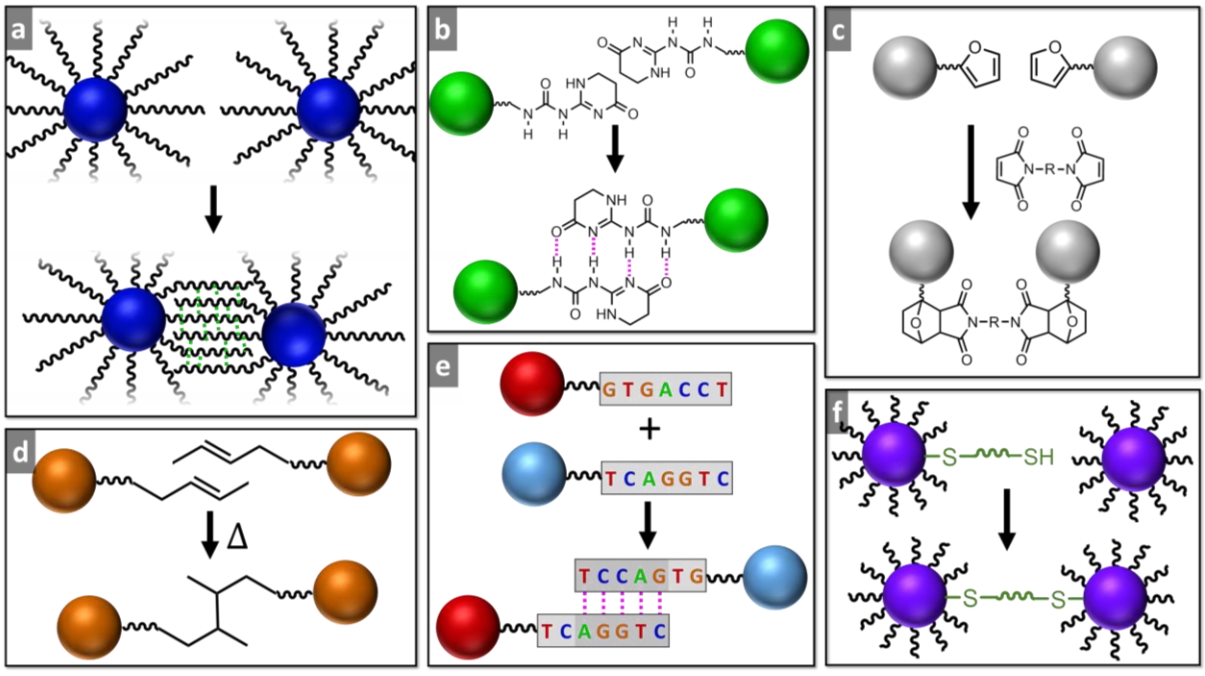

Figure 14. Exemplar inter-ligand interactions in supracrystals, a) vdW interactions from interdigitation of linear ligands, b) Hydrogen bonding between amide groups, c) Added covalent crosslinking chemical – dimaleimide diels-alder reacting with ligand-terminal furans, d) Thermal crosslinking of adjacent alkenes to form covalent bonds, e) Hydrogen bonding of base pairs in complimentary DNA strands in a binary functionalised system, f) Ligand exchange with bicapping ligand (here thiol on thiophilic metal NP).

Covalently crosslinked ligands after supracrystal assembly can form an analogue of thermoset-matrix nanocomposites; crosslinking may be achieved either directly between ligands[162] or through addition of a crosslinking chemical.[174] Covalently crosslinked systems demonstrate increased stiffness but with a more brittle failure, deforming 'granularly',[165] implying substantially fewer bonds are broken during failure and a lower toughness. Reversible crosslinking offers an alternative route towards supracrystal-wide bonding networks. These systems tend to be weaker than the covalently crosslinked systems, and susceptible to thermal cleavage at modest temperatures. Crosslinking can be performed through hydrogen bonding ligands[175] (e.g. amides, up to 12.6 MJ m^{-3}), formation of weak inter-ligand covalent bonds,[174] or through ligand substitution using ligands capable of capping multiple cores simultaneously.[176]

The reversible, reformable nature of the inter-core bonding not only improves fracture toughness and stiffness of the materials, but also introduces a degree of self-healing[175] and/or moldability[176] into the macrostructure. DNA-terminated ligands represent an interesting reversible crosslinking route, which is particularly appealing as binary DNA functionalised NPs are already used to create atypical superlattices, using NPs with complimentary 'sticky ends' to selectively bond to one another.[177] Importantly, the strength and thermal stability of the 'sticky ends' are well-established parameters and could be used to refine supracrystal (thermo)mechanical behaviour through ligand selection. However, due to their 'soft' nature, supracrystals made of DNA are expected to yield at ~0.1-1 MPa, and 50- 200% strain; comparable to thermoplastic polymers.[178] A combination of these reversible and irreversible supracrystal bonding systems has been proposed as a route to maximising both strength and toughness.[179]

Larger assemblies than as-solution-grown supracrystals are possible. Reversible crosslinking supracrystals may be physically moulded into the desired macrostructure,[175-176] and irreversibly crosslinking treatments may be applied under pressure to coalesce a powder of supracrystals into a singular crosslinked structure.[162, 164] These irreversibly crosslinked monoliths show excellent uniaxial mechanical performance, with the highest strength (630 MPa) and hardness (18 GPa) recorded for supracrystals to date. Compressive toughness is as

high as ~12 MJ m^{-3} (measured manually from provided stress-strain data).[162] Alternatively, films of supracrystals may be formed, commonly through evaporation of the initial solvent, but also through assembly at air-liquid[169] or liquid-liquid interfaces,[180] or electrophoresis.[165] While thick films may crack due to drying effects,[181] sub-micrometre thick films typically remain cohesive, with lateral dimensions on the centimetre scale routinely reported. Film thickness may be reduced to monolayer-NP thicknesses,[182] and while stiffness decreases with lowering thickness,[163] the monolayer forms a cohesive structure, exhibiting stiffness (~10 GPa) similar to that of the bulk material and strength varying with NP size (larger NPs have greater lateral inter-ligand interactions).[182] Cross-linking of supracrystal films has been shown to lead to 'crumpling' caused by shrinkage, representing a processing challenge but also illustrating the non-brittle nature of the supracrystal films at the macroscale.[180] Films are often less ordered (and thus less stiff) than respective solution-grown crystals; their lessened long-range order is intrinsically coupled to the presence of dislocations within the superlattice,[169] which are rarer in the solution grown materials.[163] The distribution of dislocations and defects may be controlled through adjusting the rate of formation,[159] with rapid formation leading to more nucleation sites and grain boundaries, and slower assembly forming larger domains, akin to typical crystal growth. However, unlike normal crystals, a 'glassier' supracrystal does not necessarily have a lower stiffness than its crystalline counterpart, as hysteresis from the rapid film formation may cause residual stress in the ligands, offsetting the decrease from lowered crystallinity.[163]

Moving forward, there is substantial room for improving the toughness of supracrystals. Through their uniaxial bonding and high degree of order, it is surprising that metal-like movement of dislocations have not been observed as a deformation mechanism, which would have provided the ideal, tuneable, non-metallic metal-replacement. Instead, the tougher materials involve polymeric ligands which lead to polymer-driven deformations, or are crosslinked, preventing core mobility during deformation. There is significant scope to better control and improve supracrystal mechanical performance, through the use of processing routes developed for optoelectronic/phononic supracrystals.[159] In particular, while non-close-packed crystal systems have been creating by using supramolecular ligand interactions,[177] non-spherical NP cores, and bi/trinary NP types, the mechanical properties of those systems have not been fully investigated yet. A further current limitation is material production scalability, which to date has been limited to the centimetre range. Larger samples are needed to truly demonstrate the translation of nanometre length scale mechanical performance to the macroscale. Finally, research in the field of supracrystals has historically focused on either

optoelectronic or mechanical properties, while the two concepts are not mutually exclusive. Recently, uniaxial tension of a supracrystal film has demonstrated visible absorption blue-shift, opening up new applications such as visual strain gauge (Figure 15),[175] and other possible complimentary mechano(opto)electronic applications.

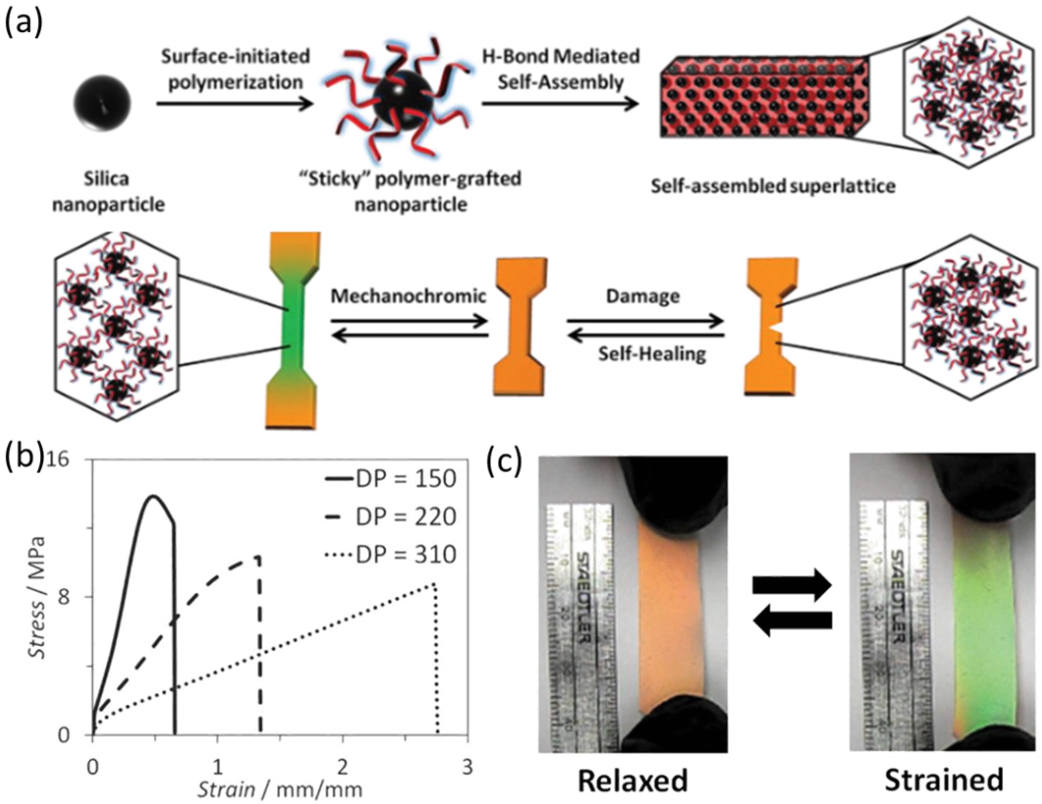

Figure 15. Mechanochromic silica NP/polyamide supracrystals (a) Schematic of NP ligand grafting and assembly, with illustration of mechanical behaviours under tension and upon damage. (b) stress-strain behaviour of materials with increasing 'degree of polymerisation' (DP) and increasing polymer chain length and decreasing NP core fraction. (c) Digital photographs of mechanochromic effect under tensile stress. Reproduced with permission from Williams *et al.*[175] Copyright 2015 John Wiley and Sons.

5. Outlook

Both historic and contemporary research into nanomaterial composites for structural materials tend to focus on maximising strength and stiffness. One material dominates much of this research: carbon fibre reinforced polymer composites. Their remarkable bulk tensile strength (*ca.* 550 – 1050 GPa) and stiffness (*ca.* 69 – 150 GPa) for a quasi-isotropic lay-up[183] coupled to low density (≤ 2 g cm^{-3}) come after substantial investment in research and infrastructure, and in the short term will remain unrivalled in real-world applications where light, strong, stiff materials are required. While outclassing carbon fibre-based FRP in strength and stiffness is a daunting prospect, its brittle failure is a significant drawback. In many structural

applications, users would prefer a lightweight material with slightly lower strength and stiffness if it were coupled to higher toughness and ductile failure. Aluminium alloys are the current main material of choice in these contexts owing to their high strength to weight ratio (≤ 700 MPa/2.7 g cm^{-3}) and potential for tough, ductile failure. Nanomaterial composites and assemblies are proving to be the ideal materials to fill this niche, combining higher strengths and lower densities than aluminium alloys. Nanomaterial-modified FRCs and carbon nanotube yarns in particular already regularly demonstrate comparable strength/stiffness to FRCs with the benefit of increased toughness. To compete with existing materials, significant capital investment is required to move these materials to industrial application; several fibre and yarn technologies have already taken steps towards scale up, owing to their ability to exploit the existing infrastructure and expertise of the polymer-fibre industries.

The greatest hurdle to be tackled arguably is not scientific or technological, but within the approach of the nanomaterials' community. It is neither feasible nor even desirable for all researchers in the field to shift focus towards improving toughness explicitly. However, we do encourage one small change which would help – reporting toughness. Most structural materials research involves tensile testing, from which it is trivial to calculate a toughness by measuring the work-to-fracture (Section 2.4). Regularly quantifying and discussing toughness even briefly will standardise it as part of the discussion around structural nanomaterials research.

Acknowledgements

AJC would like to thank the Ramsay Memorial Fellowship Trust and The Society of Chemical Industry for their funding and support. AJC, DBA, and FDL would like to thank UK Engineering and Physical Sciences Research Council (EPSRC) Programme Grant EP/I02946X/1 on High Performance Ductile Composite Technology in collaboration with the University of Bristol.

Conflict of Interest Declaration

There are no conflicts of interest to declare.

Abbreviations and symbols

B&M – Brick and Mortar; CNT – Carbon Nanotubes; CVD – Chemical Vapour Deposition; EY – Modulus; FRP – (Continuous) Fibre Reinforced-Polymer; GO – Graphene Oxide; h – Depth; l_c – Critical Length; NP – Nanoparticle; d_f – Diameter; P – Load; PVOH – Poly(Vinyl Alcohol); rGO – Reduced Graphene Oxide; RoM – Rule of Mixtures; SEM – Scanning Electron Microscope; SWCNT – Single-Walled Carbon Nanotube; vdW – van der Waals; ε_f – Strain-to-Failure; ε_y – Yield Strain; σ – Stress; σ_u – Ultimate Tensile Stress; σ_y – Yield Stress; τ_i – Interfacial Shear Strength

References

1. Jalalvand, M.; Czél, G.; Wisnom, M. R., Damage Analysis of Pseudo-Ductile Thin-Ply UD Hybrid Composites – a New Analytical Method. *Compos. Part A* **2015,** *69*, 83-93, https://doi.org/10.1016/j.compositesa.2014.11.006.
2. Ashby, M., *Materials Selection in Mechanical Design*. 2 ed.; Butterworth-Heinemann Linacre House, Jordan Hill, Oxford OX2 8DP, 1999.
3. Mallick, P. K., *Fibre Reinforced Composites: Materials, Manufacturing, and Design*. 3rd ed.; Taylor & Francis Group, LLC.: 6000 Broken Sound Parkway NW, Suite 300, Boca Raton, 2008.
4. Walsh, P. J., Carbon Fibers. *Materials Park, OH: ASM International, 2001.* **2001**, 35-40.
5. Wallenberger, F. T.; Watson, J. C.; Li, H., Glass Fibers. *Materials Park, OH: ASM International, 2001.* **2001**, 27-34.
6. Scott, A.; Mavrogordato, M.; Wright, P.; Sinclair, I.; Spearing, S., In Situ Fibre Fracture Measurement in Carbon–epoxy Laminates Using High Resolution Computed Tomography. *Compos. Sci. Technol.* **2011,** *71* (12), 1471-1477, https://doi.org/10.1016/j.compscitech.2011.06.004.
7. Mattsson, A.; Uesaka, T., Characterisation of Time-dependent, Statistical Failure of Cellulose Fibre Networks. *Cellulose* **2018,** *25* (5), 2817-2828, https://doi.org/10.1007/s10570-018-1776-5.
8. Mattsson, A.; Uesaka, T., Time-Dependent Breakdown of Fiber Networks: Uncertainty of Lifetime. *Physical Review E* **2017,** *95* (5), 053005, https://doi.org/10.1103/PhysRevE.95.053005.
9. Argon, A. S., Fracture of Composites. In *Treatise on Materials Science & Technology*, Herman, H., Ed. Elsevier: 1972; Vol. 1, pp 79-114.
10. Karger-Kocsis, J.; Mahmood, H.; Pegoretti, A., Recent Advances in Fiber/matrix Interphase Engineering for Polymer Composites. *Prog. Mater. Sci.* **2015,** *73*, 1-43, https://doi.org/10.1016/j.pmatsci.2015.02.003.
11. Gao, H.; Ji, B.; Jäger, I. L.; Arzt, E.; Fratzl, P., Materials Become Insensitive to Flaws at Nanoscale: Lessons from Nature. *Proc. Natl. Acad. Sci. U.S.A.* **2003,** *100* (10), 5597-5600, https://doi.org/10.1073/pnas.0631609100.
12. Pimenta, S.; Pinho, S. T., Hierarchical Scaling Law for the Strength of Composite Fibre Bundles. *J. Mech. Phys. Solids* **2013,** *61* (6), 1337-1356, https://doi.org/10.1016/j.jmps.2013.02.004.
13. Lee, C.; Wei, X.; Kysar, J. W.; Hone, J., Measurement of the Elastic Properties and Intrinsic Strength of Monolayer Graphene. *Science* **2008,** *321* (5887), 385-388, https://doi.org/10.1126/science.1157996.
14. Compton, O. C.; Nguyen, S. T., Graphene Oxide, Highly Reduced Graphene Oxide, and Graphene: Versatile Building Blocks for Carbon-based Materials. *Small* **2010,** *6* (6), 711-723, https://doi.org/10.1002/smll.200901934.
15. Zandiatashbar, A.; Lee, G.-H.; An, S. J.; Lee, S.; Mathew, N.; Terrones, M.; Hayashi, T.; Picu, C. R.; Hone, J.; Koratkar, N., Effect of Defects on the Intrinsic Strength and Stiffness of Graphene. *Nat. Commun.* **2014,** *5*, 3186, https://doi.org/10.1038/ncomms4186.
16. Shtansky, D. V.; Firestein, K. L.; Golberg, D. V., Fabrication and Application of BN Nanoparticles, Nanosheets and Their Nanohybrids. *Nanoscale* **2018,** *10* (37), 17477-17493, https://doi.org/10.1039/C8NR05027A.
17. Menzel, R.; Duerrbeck, A.; Liberti, E.; Yau, H. C.; McComb, D.; Shaffer, M. S., Determining the Morphology and Photocatalytic Activity of Two-Dimensional Anatase Nanoplatelets Using Reagent Stoichiometry. *Chem. Mater.* **2013,** *25* (10), 2137-2145, https://doi.org/10.1021/cm400785z.
18. Moon, R. J.; Martini, A.; Nairn, J.; Simonsen, J.; Youngblood, J., Cellulose Nanomaterials Review: Structure, Properties and Nanocomposites. *Chem. Soc. Rev.* **2011,** *40* (7), 3941-3994, https://doi.org/10.1039/C0CS00108B.
19. Clancy, A. J.; Bayazit, M. K.; Hodge, S. A.; Skipper, N. T.; Howard, C. A.; Shaffer, M. S., Charged Carbon Nanomaterials: Redox Chemistries of Fullerenes, Carbon Nanotubes, and Graphenes. *Chem. Rev.* **2018,** *118* (16), 7363-7408, https://doi.org/10.1021/acs.chemrev.8b00128.
20. Wang, W.; Dai, S.; Li, X.; Yang, J.; Srolovitz, D. J.; Zheng, Q., Measurement of the Cleavage Energy of Graphite. *Nat. Commun.* **2015,** *6*, 7853, https://doi.org/10.1038/ncomms8853.
21. Leonov, A. I., A Theory of Necking in Semi-Crystalline Polymers. *Int. J. Solids Struct.* **2002,** *39* (24), 5913-5926, https://doi.org/10.1016/S0020-7683(02)00478-X.
22. Passaglia, E., Crazes and Fracture in Polymers. *J. Phys. Chem. Solids* **1987,** *48* (11), 1075-1100, https://doi.org/10.1016/0022-3697(87)90119-3.
23. Xie, X.-L.; Mai, Y.-W.; Zhou, X.-P., Dispersion and Alignment of Carbon Nanotubes in Polymer Matrix: A Review. *Materials Science and Engineering: R: Reports* **2005,** *49* (4), 89-112, https://doi.org/10.1016/j.mser.2005.04.002.

24. Coleman, J. N.; Khan, U.; Gun'ko, Y. K., Mechanical Reinforcement of Polymers Using Carbon Nanotubes. *Adv. Mater.* **2006,** *18* (6), 689-706, https://doi.org/10.1002/adma.200501851.
25. Kinloch, A.; Shaw, S.; Hunston, D., Deformation and Fracture Behaviour of a Rubber-Toughened Epoxy: 2. Failure Criteria. *Polymer* **1983,** *24* (10), 1355-1363, https://doi.org/10.1016/0032-3861(83)90071-X.
26. Quan, D.; Carolan, D.; Rouge, C.; Murphy, N.; Ivankovic, A., Carbon Nanotubes and Core–shell Rubber Nanoparticles Modified Structural Epoxy Adhesives. *J. Mater. Sci.* **2017,** *52* (8), 4493-4508, https://doi.org/10.1007/s10853-016-0695-9.
27. Liang, Y.; Pearson, R., The Toughening Mechanism in Hybrid Epoxy-Silica-Rubber Nanocomposites (HESRNs). *Polymer* **2010,** *51* (21), 4880-4890, https://doi.org/10.1016/j.polymer.2010.08.052.
28. Ngah, S. A.; Taylor, A. C., Toughening Performance of Glass Fibre Composites with Core–shell Rubber and Silica Nanoparticle Modified Matrices. *Compos. Part A* **2016,** *80*, 292-303, https://doi.org/10.1016/j.compositesa.2015.10.036.
29. Budarapu, P. R.; Zhuang, X.; Rabczuk, T.; Bordas, S. P. A., Chapter One - Multiscale Modeling of Material Failure: Theory and Computational Methods. In *Adv. Appl. Mech.*, Hussein, M. I., Ed. Elsevier: 2019; Vol. 52, pp 1-103.
30. Ramachandramoorthy, R.; Schwiedrzik, J.; Petho, L.; Guerra-Nuñez, C.; Frey, D.; Breguet, J.-M.; Michler, J., Dynamic Plasticity and Failure of Microscale Glass: Rate-Dependent Ductile–Brittle–Ductile Transition. *Nano Lett.* **2019,** *19* (4), 2350-2359, https://doi.org/10.1021/acs.nanolett.8b05024.
31. Oliver, W. C.; Pharr, G. M., An Improved Technique for Determining Hardness and Elastic Modulus Using Load and Displacement Sensing Indentation Experiments. *J. Mater. Res.* **1992,** *7* (6), 1564-1583, https://doi.org/10.1557/JMR.1992.1564.
32. Sebastiani, M.; Johanns, K.; Herbert, E. G.; Pharr, G. M., Measurement of Fracture Toughness by Nanoindentation Methods: Recent Advances and Future Challenges. *Curr. Opin. Solid State Mater. Sci.* **2015,** *19* (6), 324-333, https://doi.org/10.1016/j.cossms.2015.04.003.
33. Greenfeld, I.; Wagner, H. D., Nanocomposite Toughness, Strength and Stiffness: Role of Filler Geometry. *Nanocomposites* **2015,** *1* (1), 3-17, https://doi.org/10.1179/2055033214Y.0000000002.
34. Xin, G.; Yao, T.; Sun, H.; Scott, S. M.; Shao, D.; Wang, G.; Lian, J., Highly Thermally Conductive and Mechanically Strong Graphene Fibers. *Science* **2015,** *349* (6252), 1083-1087, https://doi.org/10.1126/science.aaa6502.
35. Wan, S.; Peng, J.; Li, Y.; Hu, H.; Jiang, L.; Cheng, Q., Use of Synergistic Interactions to Fabricate Strong, Tough, and Conductive Artificial Nacre Based on Graphene Oxide and Chitosan. *ACS nano* **2015,** *9* (10), 9830-9836, https://doi.org/10.1021/acsnano.5b02902.
36. Ming, P.; Song, Z.; Gong, S.; Zhang, Y.; Duan, J.; Zhang, Q.; Jiang, L.; Cheng, Q., Nacre-Inspired Integrated Nanocomposites with Fire Retardant Properties by Graphene Oxide and Montmorillonite. *J. Mater. Chem. A* **2015,** *3* (42), 21194-21200, https://doi.org/10.1039/C5TA05742F.
37. Clancy, A.; Anthony, D.; Fisher, S.; Leese, H.; Roberts, C.; Shaffer, M., Reductive Dissolution of Supergrowth Carbon Nanotubes for Tougher Nanocomposites by Reactive Coagulation Spinning. *Nanoscale* **2017,** *9* (25), 8764-8773, https://doi.org/10.1039/C7NR00734E.
38. Domun, N.; Hadavinia, H.; Zhang, T.; Sainsbury, T.; Liaghat, G.; Vahid, S., Improving the Fracture Toughness and the Strength of Epoxy Using Nanomaterials–a Review of the Current Status. *Nanoscale* **2015,** *7* (23), 10294-10329, https://doi.org/10.1039/C5NR01354B.
39. Coleman, J. N.; Khan, U.; Blau, W. J.; Gun'ko, Y. K., Small but Strong: A Review of the Mechanical Properties of Carbon Nanotube–Polymer Composites. *Carbon* **2006,** *44* (9), 1624-1652, https://doi.org/10.1016/j.carbon.2006.02.038.
40. Pagani, G.; Green, M. J.; Poulin, P.; Pasquali, M., Competing Mechanisms and Scaling Laws for Carbon Nanotube Scission by Ultrasonication. *Proc. Natl. Acad. Sci. U.S.A.* **2012,** *109* (29), 11599-11604, https://doi.org/10.1073/pnas.1200013109.
41. Lee, W. J.; Clancy, A. J.; Kontturi, E.; Bismarck, A.; Shaffer, M. S., Strong and Stiff: High-Performance Cellulose Nanocrystal/poly (Vinyl Alcohol) Composite Fibers. *ACS Appl. Mater. Interf.* **2016,** *8* (46), 31500-31504, https://doi.org/10.1021/acsami.6b11578.
42. Wang, J.; Cheng, Q.; Lin, L.; Jiang, L., Synergistic Toughening of Bioinspired Poly (Vinyl Alcohol)–Clay–Nanofibrillar Cellulose Artificial Nacre. *ACS nano* **2014,** *8* (3), 2739-2745, https://doi.org/10.1021/nn406428n.
43. Huang, G.; Hou, C.; Shao, Y.; Wang, H.; Zhang, Q.; Li, Y.; Zhu, M., Highly Strong and Elastic Graphene Fibres Prepared from Universal Graphene Oxide Precursors. *Sci. Rep.* **2014,** *4*, 4248, https://doi.org/10.1038/srep04248.

44. Kobashi, K.; Nishino, H.; Yamada, T.; Futaba, D. N.; Yumura, M.; Hata, K., Epoxy Composite Sheets with a Large Interfacial Area from a High Surface Area-Supplying Single-Walled Carbon Nanotube Scaffold Filler. *Carbon* **2011,** *49* (15), 5090-5098, https://doi.org/10.1016/j.carbon.2011.07.028.
45. Boncel, S.; Koziol, K. K.; Walczak, K. Z.; Windle, A. H.; Shaffer, M. S., Infiltration of Highly Aligned Carbon Nanotube Arrays with Molten Polystyrene. *Mater. Lett.* **2011,** *65* (14), 2299-2303, https://doi.org/10.1016/j.matlet.2011.04.065.
46. HwaáLee, S.; SunáPark, J.; KyungáLim, B.; BináMo, C.; JunáLee, W.; MináLee, J.; HyungáHong, S.; OukáKim, S., Highly Entangled Carbon Nanotube Scaffolds by Self-Organized Aqueous Droplets. *Soft Matter* **2009,** *5* (12), 2343-2346, https://doi.org/10.1039/B817477F.
47. Tune, D. D.; Blanch, A. J.; Shearer, C. J.; Moore, K. E.; Pfohl, M.; Shapter, J. G.; Flavel, B. S., Aligned Carbon Nanotube Thin Films from Liquid Crystal Polyelectrolyte Inks. *ACS Appl. Mater. Interf.* **2015,** *7* (46), 25857-25864, https://doi.org/10.1021/acsami.5b08212.
48. Kimura, T.; Ago, H.; Tobita, M.; Ohshima, S.; Kyotani, M.; Yumura, M., Polymer Composites of Carbon Nanotubes Aligned by a Magnetic Field. *Adv. Mater.* **2002,** *14* (19), 1380-1383, https://doi.org/10.1002/1521-4095(20021002)14:19%3C1380::AID-ADMA1380%3E3.0.CO;2-V.
49. Lee, K. E.; Oh, J. J.; Yun, T.; Kim, S. O., Liquid Crystallinity Driven Highly Aligned Large Graphene Oxide Composites. *J. Solid State Chem.* **2015,** *224*, 115-119, https://doi.org/10.1016/j.jssc.2014.09.027.
50. Lee, W. J.; Clancy, A. J.; Fernández-Toribio, J. C.; Anthony, D. B.; White, E. R.; Solano, E.; Leese, H. S.; Vilatela, J. J.; Shaffer, M. S., Interfacially-Grafted Single Wall Carbon Nanotube/poly (Vinyl Alcohol) Composite Fibers. *Carbon* **2019,** *146*, 162-171, https://doi.org/10.1016/j.carbon.2019.01.075.
51. Miaudet, P.; Badaire, S.; Maugey, M.; Derre, A.; Pichot, V.; Launois, P.; Poulin, P.; Zakri, C., Hot-Drawing of Single and Multiwall Carbon Nanotube Fibers for High Toughness and Alignment. *Nano Lett.* **2005,** *5* (11), 2212-2215, https://doi.org/10.1021/nl051419w.
52. Huang, C.; Peng, J.; Wan, S.; Du, Y.; Dou, S.; Wagner, H. D.; Tomsia, A. P.; Jiang, L.; Cheng, Q., Ultra-Tough Inverse Artificial Nacre Based on Epoxy-Graphene by Freeze-Casting. *Angew. Chem.* **2019,** *58*, 7636-7640, https://doi.org/10.1002/anie.201902410.
53. Liu, Q.; Lomov, S. V.; Gorbatikh, L., The Interplay Between Multiple Toughening Mechanisms in Nanocomposites with Spatially Distributed and Oriented Carbon Nanotubes as Revealed by Dual-Scale Simulations. *Carbon* **2019,** *142*, 141-149, https://doi.org/10.1016/j.carbon.2018.10.005.
54. Liu, Q.; Lomov, S. V.; Gorbatikh, L., Spatial Distribution and Orientation of Nanotubes for Suppression of Stress Concentrations Optimized Using Genetic Algorithm and Finite Element Analysis. *Mater. Des.* **2018,** *158*, 136-146, https://doi.org/10.1016/j.matdes.2018.08.019.
55. Kobashi, K.; Ata, S.; Yamada, T.; Futaba, D. N.; Yumura, M.; Hata, K., A Dispersion Strategy: Dendritic Carbon Nanotube Network Dispersion for Advanced Composites. *Chem. Sci.* **2013,** *4* (2), 727-733, https://doi.org/10.1039/C2SC21266H.
56. Thakur, V. K.; Kessler, M. R., Self-Healing Polymer Nanocomposite Materials: A Review. *Polymer* **2015,** *69*, 369-383, https://doi.org/10.1016/j.polymer.2015.04.086.
57. McKee, J. R.; Huokuna, J.; Martikainen, L.; Karesoja, M.; Nykänen, A.; Kontturi, E.; Tenhu, H.; Ruokolainen, J.; Ikkala, O., Molecular Engineering of Fracture Energy Dissipating Sacrificial Bonds into Cellulose Nanocrystal Nanocomposites. *Angew. Chem.* **2014,** *126* (20), 5149-5153, https://doi.org/10.1002/anie.201401072.
58. Palmeri, M. J.; Putz, K. W.; Brinson, L. C., Sacrificial Bonds in Stacked-Cup Carbon Nanofibers: Biomimetic Toughening Mechanisms for Composite Systems. *ACS nano* **2010,** *4* (7), 4256-4264, https://doi.org/10.1021/nn100661a.
59. Shin, M. K.; Lee, B.; Kim, S. H.; Lee, J. A.; Spinks, G. M.; Gambhir, S.; Wallace, G. G.; Kozlov, M. E.; Baughman, R. H.; Kim, S. J., Synergistic Toughening of Composite Fibres by Self-Alignment of Reduced Graphene Oxide and Carbon Nanotubes. *Nat. Commun.* **2012,** *3*, 650, https://doi.org/10.1038/ncomms1661.
60. Bismarck, A.; Pfeifer, G.; Springer, J., Study on Surface-and Mechanical Fiber Characteristics and Their Effect on Epoxy Composite Properties Tuned by Continuous Anodic Carbon Fiber Oxidation. *J. Adhes. Sci. Technol.* **2000,** *14* (5), 661-690, https://doi.org/10.1163/156856100742825.
61. Mai, Y., Controlled Interfacial Bonding on the Strength and Fracture Toughness of Kevlar and Carbon Fibre Composites. *J. Matter. Sci. Lett.* **1983,** *2* (11), 723-725, https://doi.org/10.1007/BF00720414.
62. Czél, G.; Pimenta, S.; Wisnom, M. R.; Robinson, P., Demonstration of Pseudo-Ductility in Unidirectional Discontinuous Carbon Fibre/epoxy Prepreg Composites. *Compos. Sci. Technol.* **2015,** *106*, 110-119, https://doi.org/10.1016/j.compscitech.2014.10.022.

63. Narducci, F.; Lee, K.-Y.; Pinho, S., Interface Micro-Texturing for Interlaminar Toughness Tailoring: A Film-Casting Technique. *Compos. Sci. Technol.* **2018,** *156*, 203-214, https://doi.org/10.1016/j.compscitech.2017.10.016.
64. Bullegas, G.; Pinho, S. T.; Pimenta, S., Engineering the Translaminar Fracture Behaviour of Thin-Ply Composites. *Compos. Sci. Technol.* **2016,** *131*, 110-122, https://doi.org/10.1016/j.compscitech.2016.06.002.
65. Fuller, J. D.; Wisnom, M. R., Ductility and Pseudo-Ductility of Thin Ply Angle-Ply CFRP Laminates Under Quasi-Static Cyclic Loading. *Compos. Part A* **2018,** *107*, 31-38, https://doi.org/10.1016/j.compositesa.2017.12.020.
66. Leguillon, D.; Marion, G.; Harry, R.; Lecuyer, F., The Onset of Delamination at Stress-Free Edges in Angle-Ply Laminates—analysis of Two Criteria. *Compos. Sci. Technol.* **2001,** *61* (3), 377-382, https://doi.org/10.1016/S0266-3538(00)00105-6.
67. Swolfs, Y.; Verpoest, I.; Gorbatikh, L., Recent Advances in Fibre-Hybrid Composites: Materials Selection, Opportunities and Applications. *Int. Mater. Rev.* **2019,** *64* (4), 181-215, https://doi.org/10.1080/09506608.2018.1467365.
68. Longana, M. L.; Yu, H.; Jalavand, M.; Wisnom, M. R.; Potter, K. D., Aligned Discontinuous Intermingled Reclaimed/virgin Carbon Fibre Composites for High Performance and Pseudo-Ductile Behaviour in Interlaminated Carbon-Glass Hybrids. *Compos. Sci. Technol.* **2017,** *143*, 13-21, https://doi.org/10.1016/j.compscitech.2017.02.028.
69. Blaker, J. J.; Anthony, D. B.; Tang, G.; Shamsuddin, S.-R.; Kalinka, G.; Weinrich, M.; Abdolvand, A.; Shaffer, M. S.; Bismarck, A., Property and Shape Modulation of Carbon Fibers Using Lasers. *ACS Appl. Mater. Interf.* **2016,** *8* (25), 16351-16358, https://doi.org/10.1021/acsami.6b05228.
70. Greenfeld, I.; Zhang, W.; Sui, X.; Wagner, H. D., Intermittent Beading in Fiber Composites. *Compos. Sci. Technol.* **2018,** *160*, 21-31, https://doi.org/10.1016/j.compscitech.2018.03.003.
71. Karger-Kocsis, J.; Mahmood, H.; Pegoretti, A., All-Carbon Multi-Scale and Hierarchical Fibers and Related Structural Composites: A Review. *Compos. Sci. Technol.* **2019,** *186*, 107932, https://doi.org/10.1016/j.compscitech.2019.107932.
72. Qian, H.; Greenhalgh, E. S.; Shaffer, M. S.; Bismarck, A., Carbon Nanotube-Based Hierarchical Composites: A Review. *J. Mater. Chem.* **2010,** *20* (23), 4751-4762, https://doi.org/10.1039/C000041H.
73. Lubineau, G.; Rahaman, A., A Review of Strategies for Improving the Degradation Properties of Laminated Continuous-Fiber/epoxy Composites with Carbon-Based Nanoreinforcements. *Carbon* **2012,** *50* (7), 2377-2395, https://doi.org/10.1016/j.carbon.2012.01.059.
74. Garcia, E. J.; Wardle, B. L.; Hart, A. J., Joining Prepreg Composite Interfaces with Aligned Carbon Nanotubes. *Compos. Part A* **2008,** *39* (6), 1065-1070, https://doi.org/10.1016/j.compositesa.2008.03.011.
75. Kamar, N. T.; Hossain, M. M.; Khomenko, A.; Haq, M.; Drzal, L. T.; Loos, A., Interlaminar Reinforcement of Glass Fiber/Epoxy Composites with Graphene Nanoplatelets. *Composites Part A: Applied Science and Manufacturing* **2015,** *70*, 82-92, https://doi.org/10.1016/j.compositesa.2014.12.010.
76. Siddiqui, N. A.; Woo, R. S.; Kim, J.-K.; Leung, C. C.; Munir, A., Strength of Individual Hardwood Fibres and Fibre Tomode I Interlaminar Fracture Behavior and Mechanical Properties of CFRPs with Nanoclay-Filled Epoxy Matrix. *Composites Part A: Applied science and manufacturing* **2007,** *38* (2), 449-460, https://doi.org/10.1016/j.compositesa.2006.03.001.
77. Vijay Kumar, V.; Ramakrishna, S.; Kong Yoong, J. L.; Esmaeely Neisiany, R.; Surendran, S.; Balaganesan, G., Electrospun Nanofiber Interleaving in Fiber Reinforced Composites—recent Trends. *Material Design & Processing Communications* **2019,** *1* (1), e24, https://doi.org/10.1002/mdp2.24.
78. Wang, S.; Downes, R.; Young, C.; Haldane, D.; Hao, A.; Liang, R.; Wang, B.; Zhang, C.; Maskell, R., Carbon Fiber/carbon Nanotube Buckypaper Interply Hybrid Composites: Manufacturing Process and Tensile Properties. *Adv. Eng. Mater.* **2015,** *17* (10), 1442-1453, https://doi.org/10.1002/adem.201500034.
79. Grady, J. E. *Fracture Toughness Testing of Polymer Matrix Composites*; NASA Lewis Research Center, Cleveland, OH, United States: 1992; p 19930003114.
80. Rafiee, M. A.; Rafiee, J.; Srivastava, I.; Wang, Z.; Song, H.; Yu, Z. Z.; Koratkar, N., Fracture and Fatigue in Graphene Nanocomposites. *Small* **2010,** *6* (2), 179-183, https://doi.org/10.1002/smll.200901480.
81. Herceg, T. M.; Abidin, M. S. Z.; Greenhalgh, E. S.; Shaffer, M. S.; Bismarck, A., Thermosetting Hierarchical Composites with High Carbon Nanotube Loadings: En Route to High Performance. *Compos. Sci. Technol.* **2016,** *127*, 134-141, https://doi.org/10.1016/j.compscitech.2016.02.015.
82. Anthony, D. B.; Sui, X.; Kellersztein, I.; De Luca, H. G.; White, E. R.; Wagner, H. D.; Greenhalgh, E. S.; Bismarck, A.; Shaffer, M. S., Continuous Carbon Nanotube Synthesis on Charged Carbon Fibers. *Compos. Part A* **2018,** *112*, 525-538, https://doi.org/10.1016/j.compositesa.2018.05.027.

83. Zhang, X.; Fan, X.; Yan, C.; Li, H.; Zhu, Y.; Li, X.; Yu, L., Interfacial Microstructure and Properties of Carbon Fiber Composites Modified with Graphene Oxide. *ACS Appl. Mater. Interf.* **2012,** *4* (3), 1543-1552, https://doi.org/10.1021/am201757v.
84. Zhang, R.; Gao, B.; Ma, Q.; Zhang, J.; Cui, H.; Liu, L., Directly Grafting Graphene Oxide onto Carbon Fiber and the Effect on the Mechanical Properties of Carbon Fiber Composites. *Mater. Des.* **2016,** *93*, 364-369, https://doi.org/10.1016/j.matdes.2016.01.003.
85. Rutz, B. H.; Berg, J. C., Electrostatic Deposition of Silica Nanoparticles Between E-Glass Fibers and an Epoxy Resin. *J. Appl. Polym. Sci.* **2015,** *132* (8), 41516, https://doi.org/10.1002/app.41516.
86. Qian, H.; Bismarck, A.; Greenhalgh, E. S.; Shaffer, M. S., Synthesis and Characterisation of Carbon Nanotubes Grown on Silica Fibres by Injection CVD. *Carbon* **2010,** *48* (1), 277-286, https://doi.org/10.1016/j.carbon.2009.09.029.
87. Anthony, D. B.; Qian, H.; Clancy, A. J.; Greenhalgh, E. S.; Bismarck, A.; Shaffer, M. S., Applying a Potential Difference to Minimise Damage to Carbon Fibres During Carbon Nanotube Grafting by Chemical Vapour Deposition. *Nanotechnology* **2017,** *28* (30), 305602, https://doi.org/10.1088/1361-6528/aa783f/meta.
88. De Luca, F.; Sernicola, G.; Shaffer, M. S.; Bismarck, A., "Brick-and-Mortar" Nanostructured Interphase for Glass-Fiber-Reinforced Polymer Composites. *ACS Appl. Mater. Interf.* **2018,** *10* (8), 7352-7361, https://doi.org/10.1021/acsami.7b16136.
89. Liu, B.; Liu, C.; Luca, H. G. D.; Pillai, S. K. R.; David B. Anthony; Bismarck, J. L. A.; Shaffer, M. S. P.; Chan-Park, M. B., Synthesis of Epoxidized Poly(ester Carbonate)-B-Polyimide-B-Poly(ester Carbonate): Reactive Single-Walled Carbon Nanotube Dispersants Enable Synergistic Reinforcement Around Multi-Walled Nanotube-Grafted Carbon Fibers. *Polym. Chem.* **2019,** *In Press*, 10.1039/C8PY01465E, https://doi.org/10.1039/C8PY01465E.
90. De Luca, F.; Clancy, A. J.; Carrero, N. R.; Anthony, D. B.; De Luca, H. G.; Shaffer, M. S.; Bismarck, A., Increasing Carbon Fiber Composite Strength with a Nanostructured "Brick-and-Mortar" Interphase. *Materials Horizons* **2018,** *5* (4), 668-674, https://doi.org/10.1039/C7MH00917H.
91. Jackson, A.; Vincent, J. F.; Turner, R., The Mechanical Design of Nacre. *Proc. R. Soc. Lond. B* **1988,** *234* (1277), 415-440, https://doi.org/10.1098/rspb.1988.0056.
92. Sun, J.; Bhushan, B., Hierarchical Structure and Mechanical Properties of Nacre: A Review. *RCS Adv.* **2012,** *2* (20), 7617-7632, https://doi.org/10.1039/C2RA20218B.
93. Wang, R.; Suo, Z.; Evans, A.; Yao, N.; Aksay, I., Deformation Mechanisms in Nacre. *J. Mater. Res.* **2001,** *16* (9), 2485-2493, https://doi.org/10.1557/JMR.2001.0340.
94. Li, X.; Xu, Z.-H.; Wang, R., In Situ Observation of Nanograin Rotation and Deformation in Nacre. *Nano Lett.* **2006,** *6* (10), 2301-2304, https://doi.org/10.1021/nl061775u.
95. Meyers, M. A.; Lin, A. Y.-M.; Chen, P.-Y.; Muyco, J., Mechanical Strength of Abalone Nacre: Role of the Soft Organic Layer. *J. Mech. Behav. Biomed. Mater.* **2008,** *1* (1), 76-85, https://doi.org/10.1016/j.jmbbm.2007.03.001.
96. Song, F.; Soh, A.; Bai, Y., Structural and Mechanical Properties of the Organic Matrix Layers of Nacre. *Biomaterials* **2003,** *24* (20), 3623-3631, https://doi.org/10.1016/S0142-9612(03)00215-1.
97. Bonderer, L. J.; Studart, A. R.; Gauckler, L. J., Bioinspired Design and Assembly of Platelet Reinforced Polymer Films. *Science* **2008,** *319* (5866), 1069-1073, https://doi.org/10.1126/science.1148726.
98. Wang, R.; Wen, H.; Cui, F.; Zhang, H.; Li, H., Observations of Damage Morphologies in Nacre During Deformation and Fracture. *J. Mater. Sci.* **1995,** *30* (9), 2299-2304, https://doi.org/10.1007/BF01184577.
99. Barthelat, F., Designing Nacre-like Materials for Simultaneous Stiffness, Strength and Toughness: Optimum Materials, Composition, Microstructure and Size. *J. Mech. Phys. Solids* **2014,** *73*, 22-37, https://doi.org/10.1016/j.jmps.2014.08.008.
100. Barthelat, F.; Rabiei, R., Toughness Amplification in Natural Composites. *J. Mech. Phys. Solids* **2011,** *59* (4), 829-840, https://doi.org/10.1016/j.jmps.2011.01.001.
101. Zhao, H.; Yang, Z.; Guo, L., Nacre-Inspired Composites with Different Macroscopic Dimensions: Strategies for Improved Mechanical Performance and Applications. *NPG Asia Mater.* **2018,** *6*, 1, https://doi.org/10.1038/s41427-018-0009-6.
102. Tang, Z.; Kotov, N. A.; Magonov, S.; Ozturk, B., Nanostructured Artificial Nacre. *Nat. Mater.* **2003,** *2* (6), 413, https://doi.org/10.1038/nmat906.
103. Zhao, H.; Yue, Y.; Zhang, Y.; Li, L.; Guo, L., Ternary Artificial Nacre Reinforced by Ultrathin Amorphous Alumina with Exceptional Mechanical Properties. *Adv. Mater.* **2016,** *28* (10), 2037-2042, https://doi.org/10.1002/adma.201505511.

104. Das, P.; Malho, J.-M.; Rahimi, K.; Schacher, F. H.; Wang, B.; Demco, D. E.; Walther, A., Nacre-Mimetics with Synthetic Nanoclays up to Ultrahigh Aspect Ratios. *Nat. Commun.* **2015,** *6*, 5967, https://doi.org/10.1038/ncomms6967.
105. Li, Y. Q.; Yu, T.; Yang, T. Y.; Zheng, L. X.; Liao, K., Bio-inspired Nacre-like Composite Films Based on Graphene with Superior Mechanical, Electrical, and Biocompatible Properties. *Adv. Mater.* **2012,** *24* (25), 3426-3431, https://doi.org/10.1002/adma.201200452.
106. Cheng, Q.; Wu, M.; Li, M.; Jiang, L.; Tang, Z., Ultratough Artificial Nacre Based on Conjugated Cross-linked Graphene Oxide. *Angew. Chem.* **2013,** *125* (13), 3838-3843, https://doi.org/10.1002/anie.201210166.
107. Zhao, N.; Yang, M.; Zhao, Q.; Gao, W.; Xie, T.; Bai, H., Superstretchable Nacre-Mimetic Graphene/poly (Vinyl Alcohol) Composite Film Based on Interfacial Architectural Engineering. *ACS nano* **2017,** *11* (5), 4777-4784, https://doi.org/10.1021/acsnano.7b01089.
108. De Luca, F.; Menzel, R.; Blaker, J. J.; Birkbeck, J.; Bismarck, A.; Shaffer, M. S., Nacre-Nanomimetics: Strong, Stiff, and Plastic. *ACS Appl. Mater. Interf.* **2015,** *7* (48), 26783-26791, https://doi.org/10.1021/acsami.5b08838.
109. Morits, M.; Verho, T.; Sorvari, J.; Liljeström, V.; Kostiainen, M. A.; Gröschel, A. H.; Ikkala, O., Toughness and Fracture Properties in Nacre-Mimetic Clay/Polymer Nanocomposites. *Adv. Func. Mater.* **2017,** *27* (10), 1605378, https://doi.org/10.1002/adfm.201605378.
110. Chen, K.; Shi, B.; Yue, Y.; Qi, J.; Guo, L., Binary Synergy Strengthening and Toughening of Bio-Inspired Nacre-like Graphene Oxide/sodium Alginate Composite Paper. *Acs nano* **2015,** *9* (8), 8165-8175, https://doi.org/10.1021/acsnano.5b02333.
111. Wang, J.; Cheng, Q.; Lin, L.; Chen, L.; Jiang, L., Understanding the Relationship of Performance with Nanofiller Content in the Biomimetic Layered Nanocomposites. *Nanoscale* **2013,** *5* (14), 6356-6362, https://doi.org/10.1039/C3NR00801K.
112. Chen, K.; Ding, J.; Zhang, S.; Tang, X.; Yue, Y.; Guo, L., A General Bioinspired, Metals-Based Synergic Cross-Linking Strategy Toward Mechanically Enhanced Materials. *ACS nano* **2017,** *11* (3), 2835-2845, https://doi.org/10.1021/acsnano.6b07932.
113. Cheng, Q.; Jiang, L.; Tang, Z., Bioinspired Layered Materials with Superior Mechanical Performance. *Acc. Chem. Res.* **2014,** *47* (4), 1256-1266, https://doi.org/10.1021/ar400279t.
114. Wang, Y.; Li, T.; Ma, P.; Zhang, S.; Zhang, H.; Du, M.; Xie, Y.; Chen, M.; Dong, W.; Ming, W., Artificial Nacre from Supramolecular Assembly of Graphene Oxide. *ACS nano* **2018,** *12* (6), 6228-6235, https://doi.org/10.1021/acsnano.8b03025.
115. Song, P.; Xu, Z.; Wu, Y.; Cheng, Q.; Guo, Q.; Wang, H., Super-Tough Artificial Nacre Based on Graphene Oxide via Synergistic Interface Interactions of π-π Stacking and Hydrogen Bonding. *Carbon* **2017,** *111*, 807-812, https://doi.org/10.1016/j.carbon.2016.10.067.
116. Wan, S.; Xu, F.; Jiang, L.; Cheng, Q., Superior Fatigue Resistant Bioinspired Graphene-Based Nanocomposite via Synergistic Interfacial Interactions. *Adv. Func. Mater.* **2017,** *27* (10), 1605636, https://doi.org/10.1002/adfm.201605636.
117. Cheng, Q.; Duan, J.; Zhang, Q.; Jiang, L., Learning from Nature: Constructing Integrated Graphene-Based Artificial Nacre. *ACS nano* **2015,** *9* (3), 2231-2234, https://doi.org/10.1021/acsnano.5b01126.
118. Wegst, U. G.; Bai, H.; Saiz, E.; Tomsia, A. P.; Ritchie, R. O., Bioinspired Structural Materials. *Nat. Mater.* **2015,** *14* (1), 23, https://doi.org/10.1038/nmat4089.
119. Gong, S.; Wu, M.; Jiang, L.; Cheng, Q., Integrated Ternary Artificial Nacre via Synergistic Toughening of Reduced Graphene Oxide/double-Walled Carbon Nanotubes/poly (Vinyl Alcohol). *Mater. Res. Express* **2016,** *3* (7), 075002, https://doi.org/10.1088/2053-1591/3/7/075002.
120. Duan, J.; Gong, S.; Gao, Y.; Xie, X.; Jiang, L.; Cheng, Q., Bioinspired Ternary Artificial Nacre Nanocomposites Based on Reduced Graphene Oxide and Nanofibrillar Cellulose. *ACS Appl. Mater. Interf.* **2016,** *8* (16), 10545-10550, https://doi.org/10.1021/acsami.6b02156.
121. Wan, S.; Li, Y.; Peng, J.; Hu, H.; Cheng, Q.; Jiang, L., Synergistic Toughening of Graphene Oxide–molybdenum Disulfide–thermoplastic Polyurethane Ternary Artificial Nacre. *ACS nano* **2015,** *9* (1), 708-714, https://doi.org/10.1021/nn506148w.
122. Eckert, A.; Rudolph, T.; Guo, J.; Mang, T.; Walther, A., Exceptionally Ductile and Tough Biomimetic Artificial Nacre with Gas Barrier Function. *Adv. Mater.* **2018,** *30* (32), 1802477, https://doi.org/10.1002/adma.201802477.
123. Xia, S.; Wang, Z.; Chen, H.; Fu, W.; Wang, J.; Li, Z.; Jiang, L., Nanoasperity: Structure Origin of Nacre-Inspired Nanocomposites. *ACS nano* **2015,** *9* (2), 2167-2172, https://doi.org/10.1021/acsnano.5b00119.

124. Biswas, S. K.; Sano, H.; Shams, M. I.; Yano, H., Three-Dimensional-Moldable Nanofiber-Reinforced Transparent Composites with a Hierarchically Self-Assembled "Reverse" Nacre-like Architecture. *ACS Appl. Mater. Interf.* **2017,** *9* (35), 30177-30184, https://doi.org/10.1021/acsami.7b09390.
125. Hu, X.; Xu, Z.; Liu, Z.; Gao, C., Liquid Crystal Self-Templating Approach to Ultrastrong and Tough Biomimic Composites. *Sci. Rep.* **2013,** *3*, 2374, https://doi.org/10.1038/srep02374.
126. Hu, X.; Xu, Z.; Gao, C., Multifunctional, Supramolecular, Continuous Artificial Nacre Fibres. *Sci. Rep.* **2012,** *2*, 767, https://doi.org/10.1038/srep00767.
127. Zhang, Y.; Li, Y.; Ming, P.; Zhang, Q.; Liu, T.; Jiang, L.; Cheng, Q., Ultrastrong Bioinspired Graphene-Based Fibers via Synergistic Toughening. *Adv. Mater.* **2016,** *28* (14), 2834-2839, https://doi.org/10.1002/adma.201506074.
128. Zhang, J.; Feng, W.; Zhang, H.; Wang, Z.; Calcaterra, H. A.; Yeom, B.; Hu, P. A.; Kotov, N. A., Multiscale Deformations Lead to High Toughness and Circularly Polarized Emission in Helical Nacre-like Fibres. *Nat. Commun.* **2016,** *7*, 10701, https://doi.org/10.1038/ncomms10701.
129. Huang, C.; Cheng, Q., Learning from Nacre: Constructing Polymer Nanocomposites. *Compos. Sci. Technol.* **2017,** *150*, 141-166, https://doi.org/10.1016/j.compscitech.2017.07.021.
130. Peng, J.; Cheng, Q., High-Performance Nanocomposites Inspired by Nature. *Adv. Mater.* **2017,** *29* (45), 1702959, https://doi.org/10.1002/adma.201702959.
131. Han, J.-H.; Zhang, H.; Chen, M.-J.; Wang, G.-R.; Zhang, Z., CNT Buckypaper/Thermoplastic Polyurethane Composites with Enhanced Stiffness, Strength and Toughness. *Compos. Sci. Technol.* **2014,** *103*, 63-71, https://doi.org/10.1016/j.compscitech.2014.08.015.
132. Park, S.; Lee, K.-S.; Bozoklu, G.; Cai, W.; Nguyen, S. T.; Ruoff, R. S., Graphene Oxide Papers Modified by Divalent Ions—Enhancing Mechanical Properties via Chemical Cross-Linking. *ACS nano* **2008,** *2* (3), 572-578, https://doi.org/10.1021/nn700349a.
133. Zhu, H.; Zhu, S.; Jia, Z.; Parvinian, S.; Li, Y.; Vaaland, O.; Hu, L.; Li, T., Anomalous Scaling Law of Strength and Toughness of Cellulose Nanopaper. *Proc. Natl. Acad. Sci. U.S.A.* **2015,** *112* (29), 8971-8976, https://doi.org/10.1073/pnas.1502870112.
134. Sehaqui, H.; Allais, M.; Zhou, Q.; Berglund, L. A., Wood Cellulose Biocomposites with Fibrous Structures at Micro- and Nanoscale. *Compos. Sci. Technol.* **2011,** *71* (3), 382-387, https://doi.org/10.1016/j.compscitech.2010.12.007.
135. Wang, S.; Li, T.; Chen, C.; Kong, W.; Zhu, S.; Dai, J.; Diaz, A. J.; Hitz, E.; Solares, S. D.; Li, T., Transparent, Anisotropic Biofilm with Aligned Bacterial Cellulose Nanofibers. *Adv. Func. Mater.* **2018,** *28* (24), 1707491.
136. Smith, M. W.; Jordan, K. C.; Park, C.; Kim, J.-W.; Lillehei, P. T.; Crooks, R.; Harrison, J. S., Very Long Single- and Few-Walled Boron Nitride Nanotubes via the Pressurized Vapor/condenser Method. *Nanotechnology* **2009,** *20* (50), 505604, https://doi.org/10.1088/0957-4484/20/50/505604.
137. Iwamoto, S.; Isogai, A.; Iwata, T., Structure and Mechanical Properties of Wet-Spun Fibers Made from Natural Cellulose Nanofibers. *Biomacromol.* **2011,** *12* (3), 831-836, https://doi.org/10.1021/bm101510r.
138. Koziol, K.; Vilatela, J.; Moisala, A.; Motta, M.; Cunniff, P.; Sennett, M.; Windle, A., High-Performance Carbon Nanotube Fiber. *Science* **2007,** *318* (5858), 1892-1895, https://doi.org/10.1126/science.1147635.
139. Lekawa-Raus, A.; Patmore, J.; Kurzepa, L.; Bulmer, J.; Koziol, K., Electrical Properties of Carbon Nanotube Based Fibers and Their Future Use in Electrical Wiring. *Adv. Func. Mater.* **2014,** *24* (24), 3661-3682, https://doi.org/10.1002/adfm.201303716.
140. Boncel, S.; Sundaram, R. M.; Windle, A. H.; Koziol, K. K., Enhancement of the Mechanical Properties of Directly Spun CNT Fibers by Chemical Treatment. *ACS nano* **2011,** *5* (12), 9339-9344, https://doi.org/10.1021/nn202685x.
141. Naraghi, M.; Filleter, T.; Moravsky, A.; Locascio, M.; Loutfy, R. O.; Espinosa, H. D., A Multiscale Study of High Performance Double-Walled Nanotube− Polymer Fibers. *ACS nano* **2010,** *4* (11), 6463-6476, https://doi.org/10.1021/nn101404u.
142. Jung, Y.; Kim, T.; Park, C. R., Effect of Polymer Infiltration on Structure and Properties of Carbon Nanotube Yarns. *Carbon* **2015,** *88*, 60-69, https://doi.org/10.1016/j.carbon.2015.02.065.
143. Fang, S.; Zhang, M.; Zakhidov, A. A.; Baughman, R. H., Structure and Process-Dependent Properties of Solid-State Spun Carbon Nanotube Yarns. *J. Phys. Cond. Matter* **2010,** *22* (33), 334221, http://dx.doi.org/10.1088/0953-8984/22/33/334221.
144. Alemán, B.; Reguero, V.; Mas, B.; Vilatela, J. J., Strong Carbon Nanotube Fibers by Drawing Inspiration from Polymer Fiber Spinning. *ACS nano* **2015,** *9* (7), 7392-7398, https://doi.org/10.1021/acsnano.5b02408.

145. Jia, J.; Zhao, J.; Xu, G.; Di, J.; Yong, Z.; Tao, Y.; Fang, C.; Zhang, Z.; Zhang, X.; Zheng, L., A Comparison of the Mechanical Properties of Fibers Spun from Different Carbon Nanotubes. *Carbon* **2011,** *49* (4), 1333-1339, https://doi.org/10.1016/j.carbon.2010.11.054.
146. Tsentalovich, D. E.; Headrick, R. J.; Mirri, F.; Hao, J.; Behabtu, N.; Young, C. C.; Pasquali, M., Influence of Carbon Nanotube Characteristics on Macroscopic Fiber Properties. *ACS Appl. Mater. Interf.* **2017,** *9* (41), 36189-36198, https://doi.org/10.1021/acsami.7b10968.
147. Zhang, X.; Li, Q.; Holesinger, T. G.; Arendt, P. N.; Huang, J.; Kirven, P. D.; Clapp, T. G.; DePaula, R. F.; Liao, X.; Zhao, Y., Ultrastrong, Stiff, and Lightweight Carbon-Nanotube Fibers. *Adv. Mater.* **2007,** *19* (23), 4198-4201, https://doi.org/10.1002/adma.200700776.
148. Wang, J.; Luo, X.; Wu, T.; Chen, Y., High-Strength Carbon Nanotube Fibre-like Ribbon with High Ductility and High Electrical Conductivity. *Nat. Commun.* **2014,** *5*, 3848, https://doi.org/10.1038/ncomms4848.
149. Page, D.; El-Hosseiny, F.; Winkler, K.; Bain, R., The Mechanical Properties of Single Wood-Pulp Fibres. Part I: A New Approach. *Pulp and Paper Magazine of Canada* **1972,** *73* (8), 72-77.
150. Jajcinovic, M.; Fischer, W. J.; Hirn, U.; Bauer, W., Strength of Individual Hardwood Fibres and Fibre to Fibre Joints. *Cellulose* **2016,** *23* (3), 2049-2060, https://doi.org/10.1007/s10570-016-0895-0.
151. Mittal, N.; Ansari, F.; Gowda. V, K.; Brouzet, C.; Chen, P.; Larsson, P. T.; Roth, S. V.; Lundell, F.; Wagberg, L.; Kotov, N. A., Multiscale Control of Nanocellulose Assembly: Transferring Remarkable Nanoscale Fibril Mechanics to Macroscale Fibers. *ACS nano* **2018,** *12* (7), 6378-6388, https://doi.org/10.1021/acsnano.8b01084.
152. Mittal, N.; Jansson, R.; Widhe, M.; Benselfelt, T.; Håkansson, K. M.; Lundell, F.; Hedhammar, M.; Söderberg, L. D., Ultrastrong and Bioactive Nanostructured Bio-Based Composites. *ACS nano* **2017,** *11* (5), 5148-5159, https://doi.org/10.1021/acsnano.7b02305.
153. Xu, Z.; Sun, H.; Zhao, X.; Gao, C., Ultrastrong Fibers Assembled from Giant Graphene Oxide Sheets. *Adv. Mater.* **2013,** *25* (2), 188-193, https://doi.org/10.1002/adma.201203448.
154. Ceseracciu, L.; Miszta, K.; De Angelis, F.; Marras, S.; Prato, M.; Brescia, R.; Scarpellini, A.; Manna, L., Compression Stiffness of Porous Nanostructures from Self-Assembly of Branched Nanocrystals. *Nanoscale* **2013,** *5* (2), 681-686, https://doi.org/10.1039/C2NR32590J.
155. Brazhkin, V.; Lyapin, A., Hard and Superhard Carbon Phases Synthesized from Fullerites Under Pressure. *J. Superhard Mater.* **2012,** *34* (6), 400-423, https://doi.org/10.3103/S1063457612060135.
156. Dubrovinskaia, N.; Dubrovinsky, L.; Crichton, W.; Langenhorst, F.; Richter, A., Aggregated Diamond Nanorods, the Densest and Least Compressible Form of Carbon. *Appl. Phys. Lett.* **2005,** *87* (8), 083106, https://doi.org/10.1063/1.2034101.
157. Blank, V.; Popov, M.; Pivovarov, G.; Lvova, N.; Gogolinsky, K.; Reshetov, V., Ultrahard and Superhard Phases of Fullerite C60: Comparison with Diamond on Hardness and Wear. *Diam. Relat. Mater.* **1998,** *7* (2-5), 427-431, https://doi.org/10.1016/S0925-9635(97)00232-X.
158. Brazhkin, V.; Lyapin, A.; Popova, S.; Antonov, Y. V.; Kluev, Y. A.; Naletov, A., Mechanical Properties of the Superhard Polymeric and Disordered Phases Prepared from C60, C70, and C2N under High Pressure. *Rev. High Pressure Sci. Technol.* **1998,** *7*, 989-991, https://doi.org/10.4131/jshpreview.7.989.
159. Boles, M. A.; Engel, M.; Talapin, D. V., Self-Assembly of Colloidal Nanocrystals: From Intricate Structures to Functional Materials. *Chem. Rev.* **2016,** *116* (18), 11220-11289, https://doi.org/10.1021/acs.chemrev.6b00196.
160. Sanders, J.; Murray, M., Ordered Arrangements of Spheres of Two Different Sizes in Opal. *Nature* **1978,** *275* (5677), 201, https://doi.org/10.1038/275201a0.
161. Fava, D.; Fan, Y. S.; Kumacheva, E.; Winnik, M. A.; Shinozaki, D. M., Order Versus Disorder: Effect of Structure on the Mechanical Properties of Polymer Material. *Macromolecules* **2006,** *39* (5), 1665-1669, https://doi.org/10.1021/ma052470p.
162. Dreyer, A.; Feld, A.; Kornowski, A.; Yilmaz, E. D.; Noei, H.; Meyer, A.; Krekeler, T.; Jiao, C.; Stierle, A.; Abetz, V., Organically Linked Iron Oxide Nanoparticle Supercrystals with Exceptional Isotropic Mechanical Properties. *Nat. Mater.* **2016,** *15* (5), 522, https://doi.org/10.1038/nmat4553.
163. Gu, X. W.; Ye, X.; Koshy, D. M.; Vachhani, S.; Hosemann, P.; Alivisatos, A. P., Tolerance to Structural Disorder and Tunable Mechanical Behavior in Self-Assembled Superlattices of Polymer-Grafted Nanocrystals. *Proc. Natl. Acad. Sci. U.S.A.* **2017,** *114*, 201618508, https://doi.org/10.1073/pnas.1618508114.
164. Georgopanos, P.; Schneider, G. A.; Dreyer, A.; Handge, U. A.; Filiz, V.; Feld, A.; Yilmaz, E. D.; Krekeler, T.; Ritter, M.; Weller, H., Exceptionally Strong, Stiff and Hard Hybrid Material Based on an Elastomer and Isotropically Shaped Ceramic Nanoparticles. *Sci. Rep.* **2017,** *7* (1), 7314, https://doi.org/10.1038/s41598-017-07521-0.

165. Lee, D.; Jia, S.; Banerjee, S.; Bevk, J.; Herman, I. P.; Kysar, J. W., Viscoplastic and Granular Behavior in Films of Colloidal Nanocrystals. *Phys. Rev. Lett.* **2007,** *98* (2), 026103, http://dx.doi.org/10.1103/PhysRevLett.98.026103.
166. Podsiadlo, P.; Krylova, G.; Lee, B.; Critchley, K.; Gosztola, D. J.; Talapin, D. V.; Ashby, P. D.; Shevchenko, E. V., The Role of Order, Nanocrystal Size, and Capping Ligands in the Collective Mechanical Response of Three-Dimensional Nanocrystal Solids. *J. Am. Chem. Soc.* **2010,** *132* (26), 8953-8960, https://doi.org/10.1021/ja100464a.
167. Gauvin, M.; Wan, Y.; Arfaoui, I.; Pileni, M.-P., Mechanical Properties of Au Supracrystals Tuned by Flexible Ligand Interactions. *J. Phys. Chem. C* **2014,** *118* (9), 5005-5012, https://doi.org/10.1021/jp411896c.
168. Yan, C.; Arfaoui, I.; Goubet, N.; Pileni, M. P., Soft Supracrystals of Au Nanocrystals With Tunable Mechanical Properties. *Adv. Func. Mater.* **2013,** *23* (18), 2315-2321, https://doi.org/10.1002/adfm.201202563.
169. Goubet, N.; Portalès, H.; Yan, C.; Arfaoui, I.; Albouy, P.-A.; Mermet, A.; Pileni, M.-P., Simultaneous Growths of Gold Colloidal Crystals. *J. Am. Chem. Soc.* **2012,** *134* (8), 3714-3719, https://doi.org/10.1021/ja207941p.
170. Gauvin, M.; Yang, N.; Yang, Z.; Arfaoui, I.; Pileni, M.-P., Hierarchical Mechanical Behavior of Cobalt Supracrystals Related to Nanocrystallinity. *Nano Res.* **2015,** *8* (11), 3480-3487, https://doi.org/10.1007/s12274-015-0846-3.
171. Tam, E.; Podsiadlo, P.; Shevchenko, E.; Ogletree, D. F.; Delplancke-Ogletree, M.-P.; Ashby, P. D., Mechanical Properties of Face-Centered Cubic Supercrystals of Nanocrystals. *Nano Lett.* **2010,** *10* (7), 2363-2367, https://doi.org/10.1021/nl1001313.
172. He, J.; Kanjanaboos, P.; Frazer, N. L.; Weis, A.; Lin, X. M.; Jaeger, H. M., Fabrication and Mechanical Properties of Large-Scale Freestanding Nanoparticle Membranes. *Small* **2010,** *6* (13), 1449-1456, https://doi.org/10.1002/smll.201000114.
173. Choi, J.; Hui, C. M.; Pietrasik, J.; Dong, H.; Matyjaszewski, K.; Bockstaller, M. R., Toughening Fragile Matter: Mechanical Properties of Particle Solids Assembled from Polymer-Grafted Hybrid Particles Synthesized by ATRP. *Soft Matter* **2012,** *8* (15), 4072-4082, https://doi.org/10.1039/C2SM06915F.
174. Liu, L.; Yang, P.; Li, J.; Zhang, Z.; Yu, X.; Lu, L., Temperature-Controlled Cross-Linking of Silver Nanoparticles with Diels-Alder Reaction and Its Application on Antibacterial Property. *Appl. Surf. Sci.* **2017,** *403*, 435-440, https://doi.org/10.1016/j.apsusc.2017.01.162.
175. Williams, G. A.; Ishige, R.; Cromwell, O. R.; Chung, J.; Takahara, A.; Guan, Z., Mechanically Robust and Self-Healable Superlattice Nanocomposites by Self-Assembly of Single-Component "Sticky" Polymer-Grafted Nanoparticles. *Adv. Mater.* **2015,** *27* (26), 3934-3941, https://doi.org/10.1002/adma.201500927.
176. Klajn, R.; Bishop, K. J.; Fialkowski, M.; Paszewski, M.; Campbell, C. J.; Gray, T. P.; Grzybowski, B. A., Plastic and Moldable Metals by Self-Assembly of Sticky Nanoparticle Aggregates. *Science* **2007,** *316* (5822), 261-264, https://doi.org/10.1126/science.1139131.
177. Macfarlane, R. J.; Lee, B.; Jones, M. R.; Harris, N.; Schatz, G. C.; Mirkin, C. A., Nanoparticle Superlattice Engineering with DNA. *Science* **2011,** *334* (6053), 204-208, https://doi.org/10.1126/science.1210493.
178. Lequieu, J.; Córdoba, A. s.; Hinckley, D.; de Pablo, J. J., Mechanical Response of DNA–Nanoparticle Crystals to Controlled Deformation. *ACS Cent. Sci.* **2016,** *2* (9), 614-620, https://doi.org/10.1021/acscentsci.6b00170.
179. Mbanga, B. L.; Iyer, B. V.; Yashin, V. V.; Balazs, A. C., Tuning the Mechanical Properties of Polymer-Grafted Nanoparticle Networks through the Use of Biomimetic Catch Bonds. *Macromolecules* **2016,** *49* (4), 1353-1361, https://doi.org/10.1021/acs.macromol.5b02455.
180. Lin, Y.; Skaff, H.; Böker, A.; Dinsmore, A.; Emrick, T.; Russell, T. P., Ultrathin Cross-Linked Nanoparticle Membranes. *J. Am. Chem. Soc.* **2003,** *125* (42), 12690-12691, https://doi.org/10.1021/ja036919a.
181. Pileni, M. P., Supracrystals of Inorganic Nanocrystals: An Open Challenge for New Physical Properties. *Acc. Chem. Res.* **2008,** *41* (12), 1799-1809, https://doi.org/10.1021/ar800082q.
182. Qin, H.; Jin, J.; Peng, X.; Ichinose, I., Mechanical Properties of Free-Standing Single Layers of Metallic Nanocrystals. *J. Mater. Chem.* **2010,** *20* (5), 858-861, https://doi.org/10.1039/B923745N.
183. Ashby, M. F., Chapter 15 - Material Profiles. In *Materials and the Environment (Second Edition)*, Ashby, M. F., Ed. Butterworth-Heinemann: Boston, 2013; pp 459-595.

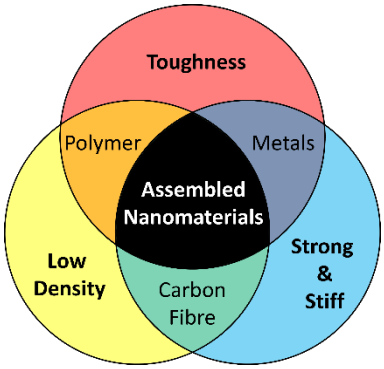

Table of Contents Figure